The Initial Position and Postural Attitudes of Driver Occupants, Posture

Raymond Brodeur
Herbert M. Reynolds
Kal Rayes
Yuntao Cui

June 21, 1996

Preface

This report is part of a larger study on the initial position and postural attitudes of driver occupants. In this report we summarize the methods for measuring and describing the posture of the seated occupant. In the vehicle laboratory we have developed the means for measuring the position of the chest, pelvis and extremities. The major goal of this section was to describe our methods for measuring joint angles and estimating the posture of the lumbar spine from chest and pelvis position measurements of the subjects. Implementing these procedures on subjects measured in our vehicle laboratory allows us to measure all joint angles of the driver occupant and estimate the posture of the subject's spine while driving a production car. Thus we can compare posture to subjective descriptions of the comfort of the car and seat. The combination of subjective comfort ratings and objective posture measurements provides an important feedback tool for the seat designer.

There are many people who contributed to this research. We would like to acknowledge and thank the personnel in Human Factors, Delphi Interior and Lighting Systems, especially Alicia Vertiz, M.D., Director of Human Factors, for her support in this research. There are many at ERL we would like to thank, including Bill Dinnan, Robert Kerr, Ben Moeggenberg and Doug Neal for the many hours involved with designing and building much of the equipment described in this report. We would also like to thank Maria Eppler for her assistance with data collection and for her organizational skills and Lanelda Kelson for her secretarial assistance.

Finally, we would like to express our appreciation to the faculty and staff at Michigan State University who have been involved in this research for the past several years. We would like to thank George Stockman, Ph.D., Computer Science, and his students for their help in developing the 3DAQ software. We would also like to thank the people in Purchasing, Contracts and Grants and other departments within the University who have supported this program in their respective roles at the University.

Table of Contents

List of Figures

List of Tables

The Initial Position and Postural Attitude of Vehicle Operators:
Posture

ABSTRACT

The posture, pressure and subjective responses of forty subjects (20 male, 20 female) were measured during two highway drives. Four video cameras were used to measure targets on each subject in addition to measuring EMG and pressure in the seat cushion and the seat back using pressure mats. Subjective questions were asked at specific time intervals or if the subject adjusted the seat or indicated they were feeling uncomfortable. The goal of this research was to compare the objective measurements to the subjective comfort responses of the subjects. In this report we describe the posture of the subjects during two different highway drive tests. During the fixed back drive, the seatback angle was controlled at a 15^o or 30^o back angle, in random order, with subjects able to control all adjustments on the 12-way power seats except back angle. During the free comfort drive, subjects had full control over all of the 12 adjustments (6-way power seat, 4-way lumbar support, 2-way back angle). We found that compared to the SAE seat design template, Oscar, all subjects sat with their hip joints significantly forward of the H-point and that the point of maximum deflection (D-point) for the subjects was further forward and with less penetration than that of the design template. Both males and females sat with similar torso-thigh angles as that of the design template, but males sat with a more reclined posture than females and with larger elbow angles. Compared to the design knee angle, both males and females were significantly less than that of Oscar, with males having an even smaller angle than females. Most males had the seat at the full rear-ward position, which was probably a factor in their knee angle. The reclined (30^o) seatback angle resulted in the most upright posture, but we strongly suspect that this was maintained with significant muscle activity in order to position the back and head to operate the vehicle.

The Initial Position and Postural Attitude of Vehicle Operators:
Posture

I. Introduction

The position of the human operator has been the most important parameter in vehicle package accommodation for many years. For example, OSCAR, the SAE two-dimensional template, is used as the primary design tool for seats and packages although it was not designed nor intended for use in the design of seats. The geometry represented by OSCAR is purely positional with no real attempt on the part of the SAE committee responsible for developing this tool to represent human posture in this 2D template. Within the biomechanical and ergonomic literature, however, posture has been identified as a parameter that needs considerable attention in the design of seats and control locations. With the development of technology to take measurements of the motor vehicle operator on the highway, the position and posture of the human operator can be empirically studied. These new data can be used to design seats in different vehicle packages to support healthy postures in the vehicle operator.

Posture of the vehicle operator has been a theoretical parameter in seat design for many decades. Many designers and engineers have thought, for example, that to support the occupant in an erect posture, a lumbar support must be present in the seat back. The contour of the seat has also been used to suggest that posture was an important feature of the seat design. However, posture is defined by the relative orientation of motion segments in the human body and subsequently the seat must be very carefully designed so that the occupant can sit in a desired posture with seat support rather than muscle activity. The goal of a good seat is to provide a structural system that supports the occupant in preferred postures and the ability to sit in that posture without muscle fatigue. Thus, the quality of a seat to support "good" posture has two empirical tests:

1) Can the occupant get into the desired posture?
2) Can the occupant stay in the desired posture without significant muscle activity?

These questions are only answered from measurements of people seated in the vehicle while it is on the highway, either as passenger or driver. In the current investigation, we have studied only the driver and developed a methodology to quantitatively describe posture of the driver while operating the vehicle on the highway.

A. Review of Critical Postural Problems in Seated Automotive Occupant

In order to illustrate the relationship between occupant posture in the seat and seat design in the vehicle, a review of the literature on seated posture and their representation in the tools of seat design is needed. There are several areas in which light on this problem can be shed by reference to the literature, although the literature doesn't offer results that define the appropriate design criteria. This body of literature concerning biomechanics, ergonomics, back pain and comfort simply leads to the directions followed in the analysis of the data in this report.

In general, erect posture is defined by a forward rotation of the pelvis and an accompanying lordotic curve of the lumbar spine. In contrast, a slumped posture is defined by a rearward rotation of the pelvis and an accompanying kyphotic curve of the lumbar spine. However, when sitting, the pelvis rotates rearward and the lumbar spine tends to flatten. When standing, the pelvis rotates forward and the lumbar spine tends to become lordotic (thus the s-shaped curve of the spinal column seen in anatomical texts). Thus, the erect sitting posture is not a natural consequence of sitting. As a result, several investigators have suggested that a lumbar support is needed to help the body maintain what is considered the more healthy posture, erect sitting with a lordotic lumbar spine.

Andersson [1] claims that an erect posture reduces electrical activity in the muscles around the spinal column and reduces the pressures in the intervertebral discs as they transmit the load of body weight through the spinal column. In contrast, Adams and Hutton [2] point out, however, that the erect posture may lead to more osteoarthritis in the facet joints and the slumped posture may lead to more annulus ruptures (i.e. a ruptured disk). In contrast to Andersson, Adams and Hutton propose that a neutral posture is the best for sitting and lifting tasks.

Hall [3], however, points out some years prior to the research previously discussed that good ergonomic seat design provides support for drivers to vary their posture. In addition to this capability in the design, joint angles should be optimally at their mid-range position. Other suggestions that occur in the ergonomic literature concern the ability of the worker to vary their position from sitting to standing throughout the period of activity. Epidemiological research by Heliövaara [4] and Kelsey [5] on the incidence of back pain and back problems leading to hospitalization among professional drivers would support the need for this change in position and posture in drivers. That is, they found that the severity of back pain increases with increased length of time in the sitting position. Thus, the basic principle that appears to be violated in automotive seating is the inability of the occupant to easily change posture in the seat while still maintaining a functional position relative to the controls and vision requirements to operate the vehicle.

Troup [6] pointed out that sitting increases stress on the spinal column. He identified four causes of the mechanical stress: (1) postural stress; (2) vibratory stress; (3) muscular effort; and (4) shock or impact. In a very thorough review of the literature, he found ample evidence to support these four mechanical factors as being highly likely to be the major contributing factors to back pain. In today's automobiles, all four are possible, but postural stress and muscular effort are the most likely mechanical causes of back pain among drivers. As the suspension systems improve in both the vehicle and seat, the effects of vibration and impact/shock should diminish on the driver and passenger. However, there is a relationship between posture and muscle activity independent of the driver operating the vehicle.

Postural muscles in the back are used to maintain an erect posture in standing and unsupported sitting. However, in the motor vehicle, the driver can recline against the seat back and rest these postural muscles. Thus, the effect of muscle activity on the back should be minimized in a seat that supports the back in a reclined position. Andersson et al [7] and Hosea et al [8] found that muscle activity is associated with seat inclination and lumbar support. In general, they found that a seat back reclined 120º with 5cm of lumbar support (normal to the plane of the seat back) minimizes muscle activity and correspondingly disc

pressure. Activities such as depressing the brake pedal or clutch increase back muscle activity but most vehicles today are sold with automatic transmission and power brakes that require less effort to operate. Thus, muscle activity would be primarily used to move the body into position and/or to hold the body in a position that is not supported by the seat.

Reed et al [9] conducted an extensive review of this literature and concluded that the geometric fit between the occupant and seat is the most easily accommodated and may result in the greatest improvement in seat comfort when compared to "feel' and "support" parameters. These latter parameters primarily describe pressure distribution and contours respectively in the seat. Reed et al expresses the opinion that seat comfort is comprised of fit, feel and support between the occupant and seat. They point out, however, that more study of the actual seat/occupant interaction is needed to make significant improvements from what has been recommended for the past fifty years. In general, their review failed to include the substantive role the seat suspension system (i.e. foam, springs, upholstery) plays in the support of the seated occupant. They further failed to recognize the need to measure the position of the occupant's skeletal structure in the investigation of the fit, feel and support in the seat. Their summary clearly points to the need for seats that support not only the variety of body sizes in the driving population, but also the variety of postures within a single driver in the population. In general, however, they seem to feel that there is inadequate data at present to successfully meet these two goals.

The basic design criteria for accommodating diversity in the driver population have concentrated on the position and range of movement of H point rather than including posture. H-point, a critical landmark in seat and package design, describes the location of the hip joint in the two-dimensional SAE template, commonly referred to as OSCAR. This landmark has been used with the location of the heel and eye to represent the position of the vehicle operator since the development of OSCAR in the late 1960's. The 2D template is based upon the combination of data from three sources: Geoffrey [10], Dempster [11], and Stoudt et al [12]. Unfortunately, this landmark has been mechanically used as the pivot for the torso rather than the pivot for the thigh. Since the torso is not a rigid body, there are many pivot points in the torso. For seat design, the most important pivot point, however, is the pivot point for the pelvis since it lies at the location of the greatest load-bearing region in the seat. The pivot for the pelvis is under the ischial tuberosities [13,14] and these structures are the anatomical equivalent to the SAE D-point defined by OSCAR as the point of greatest deflection in the seat cushion. Thus, through faulty biomechanical reasoning in the design of OSCAR, the relationship between posture and position has been distorted.

The significance of this error can be seen in how the relative orientation of the pelvis controls the amount of curvature in the low back. Many investigators have reported this coupling phenomenon [15,16,17]. The relative orientation of the pelvis, however, is not enough unless the seated occupant can relax in that position. Nachemson [18] investigated how the curvature of the lumbar spine is stabilized. The skeletal system moves as a result of muscle contraction or the force of gravity acting on the passive body. When a person sits in an upright posture without support, only muscle activity is available to stabilize the curvature of the spine against the force of gravity. Nachemson found that the psoas muscle is a primary stabilizing force in this activity, whether the person is sitting in a slumped or erect posture. That is, if a seated operator sits erect, muscle activity stabilizes this posture unless proper support in the seat is available. Likewise, if a seated operator sits

in a slumped posture, proper support in the seat is necessary to minimize the level of muscle activity to maintain this posture. As a result, the design of seats to support the body in different postures defined by the relative orientation of body segments in the seated person requires a design that considers not only the size and shape of the body, but also the location of the body's segments in the seat.

The most critical point in defining the location of the body in the seat is D-point. In this context, however, D-point is the ischial tuberosity, not the point on OSCAR that represents the greatest deflection of the seat cushion. D-point is the location of the greatest pressure in the seat and the greatest deflection of the seat. These parameters describe the location of the point at which the greatest proportion of body weight is transmitted into the seat cushion. As stated previously, D-point in this new definition is the location of the pelvic pivot point that is a critical point in defining pelvic orientation and consequently lumbar curvature.

In contrast to the relationship of D-point to the seat, H-point is one of the most critical points in defining the location of the body in the vehicle. Associated with H-point is the location of the eye and heel that in combination are used to define packaging of the occupant in the automobile environment [19]. The tools that have been established for this packaging activity have also been used for seat design. SAE documentation of these tools clearly states that they are "...not to be construed as instruments which measure or indicate occupant capabilities or comfort" (p 34.[27, 20]). Despite this admonition to the contrary, all seat designers use these tools for lack of something better. The two-dimensional template is used to design the seat and the three-dimensional H-point machine is used to evaluate the seat. Neither of these tools correctly estimates the shape of the back nor include any postural data that assists the design in comfort and health design decisions. The scientific basis of these tools rests on previously mentioned work by Geoffrey [10], Dempster[11], and Stoudt et al.[12].

Comfortable joint angles, on the other hand, are based upon theoretical recommendations by Rebiffe [21] and Babbs [22] along with the empirical experience of the packaging engineer. These angles are primarily for the joints in the arms and legs and they correspond interestingly to a prediction of joint angles under weightlessness conditions by Kennedy in 1964 [23]. These joint angles all lie near the mid-range position of each joint. There are, however, no numerical recommendations for the orientation of the motion segments in the spine. Several authors [13,24] have recommended the erect posture of the spinal column and comfort while others [2,16] have recommended a neutral posture of the spinal column for comfort and health.

In conclusion, the posture of the vehicle operator is an important parameter in the design of the vehicle interior and seat. The human body is extremely adaptable, but as we have learned from the ergonomic lessons of the 20th century, it is also easily harmed by the abuse of this adaptability in product design. Thus, it is important to study the functional posture as well as the "functional anthropometry" [19] of the human vehicle operator. Since this has been defined as an important problem that needs investigation, we must consider when during the operator's time behind the wheel is the appropriate period of study. There is a clearly defined difference between the "showroom" and "driver" opinions of vehicle performance and comfort. With this distinction, we need to identify in a research

environment, the equivalent period of time to "driver" behavior that can serve as the time period during which we investigate the vehicle operator's posture.

B. Modal Position in Seat and Occupant Posture

Real drive situations produce stress on the vehicle operator to maintain an appropriate functional position and posture to drive the vehicle. In a seat buck, there are no consequences for moving out of a driving position, and the level of alertness is much lower for the driver. Posture and position relative to seat support should provide a "relaxed" driver who can concentrate on operational activities in the vehicle. As a result, a real driving laboratory [25] is necessary to study operator position and posture under real-life conditions that produce their own levels of stress on the operator to perform at a normal and safe level of vehicle operation.

Since real drive situations occur over time, it is necessary to define a period of time during which occupant posture will be investigated. It is impractical to investigate driver posture continuously and there are apparently different cycles to the driving period that need to be considered. For example, if a vehicle operator is behind the wheel of a new vehicle that he/she has not driven before, there is a period of acclimation that must be considered. That is, the driver must become accustomed to the idiosyncrasies of the vehicle and it takes a period of time to learn where the optimal seat position is located for each driver. After this initial acclimation period is over, we assume that the driver behaves in a representative manner regarding seat position and his/her posture in the seat. To define the period of time that we want to measure the optimum level of comfort the driver experiences relative to the vehicle package, we define a modal position.

The modal position is defined as the longest period of time during which the seat is not adjusted [25]. The time from beginning to end of the modal position is the modal period. The data to define posture were measured at the beginning and end of the modal position. Thus, the original question regarding the position of the occupant in the seat can be investigated relative to the posture of the occupant at the beginning and end of the modal period. The change in posture from beginning to end is an approximation of the ability of the occupant to remain in their preferred position but it does not document the time-based history of changes that occurred from the beginning to the end of the modal period. Since some of the drivers had a modal period of 60 minutes, the change recorded in two measurements does not adequately document the history during the modal period. To investigate the history of body movement in and out of the seat during the modal period, a continuous video recording was made and analyzed with the results reported in the technical report on driver comfort [26].

The relationship between modal position of seat and occupant posture is defined by the two separate conditions: joint angles in the leg and spinal posture in the torso. These two parameters define body segment positions between heel, h-point and eye--the functional driver landmarks necessary for proper occupant packaging in the vehicle. Between heel and H-point are two joints and two links that should be positioned in or near to their mid-range joint position for comfort and health. Between H-point and eye lies the pelvis and spinal column. The models of spinal posture and pelvic orientation clearly define geometric relationships that can increase or minimize the stress on the soft tissue that holds the eye in

the driving position defined within the SAE "eyellipse." The relationship between seat position and occupant posture crosses the boundary between functional measurements of preferred occupant position of the seat and the preferred occupant posture in the seat as measured by biomechanical representations of the skeletal linkage system and occupant comfort. The task for the present investigation was therefore to link these two sets of measurements to describe the position of the occupant and the change of position of the occupant as he/she experienced comfort or discomfort in the seat while driving the vehicle.

C. Problems for the present report.

As described in the previous sections, the most healthy seated postures are considered to be either erect or neutral. The question for any investigation of driver posture is then to measure the posture of the driver. Thus, does the driver sit in either an erect or neutral posture? This question differs from whether the occupant can get into his/her preferred posture in the seat. Furthermore, it raises a very subjective question regarding whether the seat design should only support one posture or should it be designed to support multiple postures. However, for the present report, the first task is simply to document the posture that each subject is sitting. To document this posture, we will present joint angles, pelvis orientation, D-point and H-point locations, and lumbar curvature.

Joint angles are defined by the included angle between adjacent skeletal links. Video anthropometry measurements are made of targets on the body's skin surface over palpable landmarks on the arms and legs. These landmarks are well defined but they contain a bias since the landmarks are not inside the joint. For joint angles, however, it is assumed that this bias is negligible and the angle is a close approximation of the joint angle.

Pelvis orientation largely determines lumbar curvature and is measured in the present study with data from a pressure mat and video anthropometry [27]. We locate the occupant's D-point and H-point from external body measurements. The pelvic ischium (i.e. the anatomical equivalent to D-point) on the pressure mat defines the location of the pelvis in the XY plane. We locate the anterior superior iliac spine (ASIS) in the video anthropometry data to define the location of the pelvis in the XZ plane. H-point is calculated from a model based upon the relationship between ASIS and pelvic ischium. D-point is defined as the greatest concentration of pressure under the buttocks. We estimate lumbar curvature using a model of the spine described in the spinal report [42].

These parameters are investigated to describe posture at the beginning and end of the modal period. Changes in posture between these two measurement events represent the only quantitative change in posture we measured. We investigated body motion (i.e. body language) during the modal period to evaluate the change in posture hypothesis and its relationship to comfort [28]. The results of the investigation into body movements during the modal period are presented in the technical report on comfort [26].

By collecting data on drivers operating the vehicle on the highway, we created a reverse engineering problem. Seats are designed around the SgRP in a manufacturer's design position. Drivers, on the other hand, use the seat where it best fits their geometric needs in the vehicle package. As a result, reporting the data in an external axis system includes the displacement of the seat that accommodates differences in body size and preference in the driver population. To mathematically remove these extraneous driver

effects from the data so that the results are comparable to the original design, we used a reverse engineering procedure to physically measure the seat and transform its location for each operator back to the design position. As a result, we created a design window that reports the range of positions used by the 40 driver subjects and defined a range of variation about the design position that describes how well the H-point machine estimates the actual position of H-point in the driver. The same information was needed to estimate the location of D-point in the driver for comparison with the location of D-point by OSCAR. The results are presented so that comparable data are available to the designer as well as for future studies of different vehicle packages.

II. Methods

A. Equipment, Subjects and Data Collection Procedures

We selected 40 subjects according to their age, sex, and stature to drive in this investigation of driver position, posture and comfort. Each subject drove the vehicle three times. The first drive was a 20-minute acclimation drive for the subject to become accustomed to the vehicle, ride tech, instrumentation, and clothing. We controlled back angle in the second drive with a reclined back angle of 30º and an upright back angle of 15º (fixed back drive). For the third and last drive, each subject had complete control of the 12 power features in the seat (free comfort drive). The seat was an AM6 W seat with a six-way power adjuster, four-way power lumbar, and a two-way power recline. The ride tech sat in the back seat (right rear) and operated the computer that was used to collect data during the drive while the driver operated the vehicle.

We collected data from video cameras, pressure mats, position and angular transducers in the seat, and electromyography (EMG) electrodes attached to the subject's back. The video anthropometry system consists of an array of video cameras used to measure the location of targets on a subject while they drove the automobile [29,30]. The pressure mats were placed under the upholstery in the seat back and cushion [29]. Seat position transducers were attached to the power memory cables [25]. The position of the EMG electrodes is described in the experimental protocol report [29].

All data were collected according to either a fixed protocol or when the driver adjusted the seat. The fixed protocol specified that the data be collected at 0, 30, 45 minutes of each of two legs of the fixed back drive and at 0, 30, 90, and 120 minutes on the free comfort drive. If the driver adjusted the seat after the 30 minute data collection time, then the ride tech was to collect data and wait until the seat was adjusted again, 60 minutes or the end of the drive, whichever came first. The reduction of all data has been described in previous reports [25,29,30].

B. Data Analysis

1. Video Anthropometry System

The video anthropometry system utilized four video cameras strategically located on the passenger side of the vehicle to fully record the complete outline of each driver, without regard to body size or seat position in the vehicle. Each camera had a 4.8mm auto-iris lens, a notch IR filter, and an IR LED system that was turned on when the images were collected. This video system was developed for this study and utilized software to digitize the images developed at MSU in the Department of Computer Science for this project [29,30]. Images from all four cameras were collected at specified times, either according to the protocol or by occupant seat movement, and stored on a hard disk for off-line analysis in the laboratory.

The total number of images, the number of useable images and the number of targets that could be used were analyzed to determine sources of problems that lead to either poor image quality and thus loss of data or problems that resulted in the loss of specific targets. For example, when driving under an overpass, the camera irises open, thus an

image set taken immediately after the car is through the overpass is overexposed, making those images useless. The ride-techs decided if image quality was sufficient; however, they had to view the image on an LCD screen that did not adequately represent the image quality. The ride-techs were usually able to determine over or under exposure and re-take the image. However, they usually could not identify individual retro-reflective targets on the LCD monitors. For example, the shoulder belt often covered the chest targets leading to a loss of data for those landmarks. Since individual targets were usually not visible on the LCD images, the ride-techs often did not recognize these as missing targets.

The errors of the video anthropometry system were analyzed in three ways. The absolute error of the camera measurement system was determined by using the video system to measure the 3-D positions of 69 known points within the field of view of the camera array [11]. The results of this error analysis are summarized in the results section. We also investigated the difference between three trained individuals locating the same retro-reflective targets on the same set of images. Since the true positions of the targets were not known, the measurements errors were estimated by comparing the Euclidean distances between retro-reflective targets. In addition we examined the consistency of locating the same retro-reflective targets on a subject but at different time frames. Again, the true positions of the targets were not known; thus, we estimated the errors by comparing the Euclidean distance between sets of two targets that were both attached to the same rigid body (for example, the distance between the knee target and ankle target).

2. Pressure Mat Data

Equipment

Pressure Mats. Two types of Tekscan pressure mats were used. A 381mm x 457mm mat with 5mm x 5mm sensors on 10mm centers was used to measure pressure in the automobile seat. The upholstery on the driver seat was modified so that the large Tekscan pressure mat could be placed between the foam and the upholstery so that subjects could not see or feel the pressure mat. Two smaller pressure mats were used to measure the pressure of subjects seated on a hard seat. The smaller pressure mats were 112mm x112mm with 1.2mm x 1.2mm sensors on 2.5mm centers. The two fine-grid pressure mats were fixed to a hard seat so that when a subject was seated, one pressure mat would lie below each ischial tuberosity. The smaller pressure mats allowed a more exact measurement on the inter-ischial tuberosity distance for each subject. The inter-ischial tuberosity distance is required for the semi-automated detection of the ischial tuberosities on the larger pressure mat.

Data analysis procedures

Fine-Grid Pressure Mat Data on the Hard Seat. The pressure data from the fine-grid pressure mats was concentrated under the ischial tuberosities due to the fact that the subjects were seated on a hard seat. The pressure pattern consisted of a high-pressure plateau surrounded by a relatively steep pressure drop in all directions. We assumed that the ischial tuberosities were located at the centroid of the largest closed region of high pressure values.

The pressure data was smoothed using a Gaussian mask to remove the effects of isolated high pressure points. All data below a threshold of 50% of the maximum value was removed. The largest connected component was assumed to be the area of contact with the ischial tuberosity. The centroid of the largest connected component on each mat was assumed to be the best estimate for the location of the ischial tuberosity.

The distance between ischial tuberosities was computed by knowing the distances between the pressure mats and the distances between each cell of the pressure mats. The inter-ischial tuberosity distances for our subjects were compared to data available in a data base described by Reynolds, *et al* [42].

Large Pressure Mat on a Soft Seat.

The large pressure mat has a coarse pressure grid (10mm x 10mm) and thus the corresponding pressure map requires smoothing and interpolation. We accomplished this by using a bivariate interpolation technique, described below.

Bivariate Interpolation. In this section we describe our approach for reconstructing a smooth surface from arbitrary triangulations of unorganized 3D points using a bivariate surface reconstruction method. The interpolating function on each triangle is a fifth-degree polynomial. The approach preserves the advantages of Garcia's [44] approach and has the advantage that the reconstructed surface has C^1 continuity across the boundaries of neighboring triangles. Interpolation of *z* values in a triangle by a bivariate fifth-degree polynomial in *x* and *y* was first used by Akima [45]. Our approach differs from Akima's for two reasons: First, we compute the triangular mesh using an efficient incremental algorithm [46]. This triangulation scheme can handle an arbitrary number of unorganized 3D points. Second, we improve the accuracy of the estimation of the partial derivatives using least squares fitting.

A triangular mesh is obtained by applying an efficient incremental algorithm described previously [46], the problem of surface reconstruction is transformed into a smooth approximation of the irregular triangular mesh for the control points.

Let Ω be a simply or multiply connected bounded domain in the (x_1, x_2)-plane with the boundary Γ. Γ consists of a finite number of simple closed polygons Γ_i (i=0,...,r); Γ_1, Γ_2, ... Γ_r lie inside Γ_0 and do not intersect. Let $M = \{ \overline{T}_\lambda \}$ be a triangulation of the set $\overline{\Omega} = \Omega \cup \Gamma$, i.e. a set of a finite number of triangles having the following properties: open triangles are disjointed, the union of closed triangles is $\overline{\Omega}$ and any two adjacent triangles have either a common vertex or a common side.

Let us consider a triangle T with vertices P_1, P_2, P_3. Let $p(x_1, x_2)$ be a fifth degree polynomial:

$$p(x_1, x_2) = \sum_{i=1}^{5} \sum_{j=0}^{5-i} a_{ij} x_1^i x_2^j \qquad (1)$$

To determine such a polynomial we need 21 conditions. We choose them in the following way:

- The values of the function and its first-order and second-order partial derivatives are given at each vertex of the triangle. This yields 18 independent conditions.
- The partial derivative of the function differentiated in the direction perpendicular to each side of the triangle is a polynomial of degree three, at most, in the variable

measured in the direction of the side of the triangle. Since a triangle has three sides, this assumption yields three additional conditions.

It can be shown that the interpolated values are C^1 continuous across the boundaries of neighboring triangles [45].

Estimation of Partial Derivatives. The partial derivatives at each vertex of the triangular mesh are estimated using orthogonal polynomials. Two-dimensional discrete orthogonal polynomials are constructed over the neighborhood of each vertex. The partial derivatives are then derived based on these polynomials.

The discrete orthogonal polynomial basis set of size *N* has polynomials from degree zero through degree *N*-1 [47]. Let $P_n(r) = r^n + a_{n-1}r^{n-1} + \ldots + a_1 r + a_0$ be the *n*th order polynomial. $P_n(r)$ can be constructed if $P_0(r) \ldots P_{n-1}(r)$ have been defined. $P_n(r)$ must be orthogonal to each polynomial $P_0(r) \ldots P_{n-1}(r)$. Hence we have the *n* equations

$$\sum P_k(r)(r^n + a_{n-1}r^{n-1} + \ldots + a_1 r + a_0) = 0, \quad k = 0, \ldots n-1 \tag{2}$$

The unknowns $a_0, \ldots, a_{n-1}$ can be obtained after solving the above linear equations. Two-dimensional discrete orthogonal polynomials can be created from two sets of one-dimensional discrete orthogonal polynomials by taking tensor products.

Next, we construct two-dimensional discrete orthogonal polynomials over a neighborhood. Let *R* and *C* be index sets satisfying the symmetry condition $r \in R$ implies that $-r \in R$ and $c \in C$ implies that $-c \in C$. We assume in each neighborhood of (*R, C*), the pressure distribution takes the form of the sum of the two-dimensional discrete orthogonal polynomials $\{P_0(r,c), \ldots P_{N-1}(r,c)\}$.

For each pair (*r,c*), where $r \in R$ and $c \in C$, let a pressure value *f(r,c)* be observed. The exact least squares fitting problem is to determine coefficients $k_0,\ldots,k_{N-1}$ such that

$$e^2 = \sum_{(r,c)\in(R,C)} (f(r,c) - \sum_{i=0}^{N-1} k_i P_i(r,c))^2 \tag{3}$$

is minimized. The solutions are

$$k_i = \frac{\Sigma_{r\in R, c\in C} P_i(r,c) f(r,c)}{\Sigma_{r\in R, c\in C} P_i^2(r,c)} \tag{4}$$

Each k_i is a linear combination of the pressure values. Appendix A shows the kernels for estimating the coefficients $k_1, k_2,\ldots,k_{10}$ of the bivariate cubic:

$$\begin{aligned} d(r,c) = {} & k_1 + k_2 r + k_3 c + k_4(r^2 - 2) + k_5 rc + k_6(c^2 - 2) \\ & + k_7(r^3 - 3.4r) + k_8(r^2 - 2)c + k_9 r(c^2 - 2) + k_{10}(c^3 - 3.4c) \end{aligned} \tag{5}$$

in a 5 x 5 neighborhood [48]. Once the fitting coefficients have been computed, the estimate for any derivative at any point can be obtained. In Appendix B we show that by

controlling how the triangulation is refined, the approximate solution converges to the exact solution.

Locating the Ischial Tuberosities

Our method for locating the ischial tuberosities from the smoothed coarse-grid pressure mat data is a semi-automated technique that requires the inter-ischial tuberosity distance obtained from the hard seat measurements. The pressure data from the large pressure mat is first smoothed using the methods described above. The smoothed pressure surface is then interpolated onto a 1mm X 1mm grid and the resulting data stored in an image format (PGM) for later analysis.

The smoothed and interpolated pressure data was displayed in a gray-scale (0-255) format, with high pressure corresponding to white. Software was developed for locating the peaks in a user-defined area of interest. A best estimate of the area containing each of the ischial tuberosities was outlined. All local peaks within each of these areas were determined based on the sum of the first partial derivatives of the pressure surface at each point. Under ideal conditions, the local peaks within the outlined areas were highlighted and the two peaks that most closely matched the inter-ischial tuberosity distance measured in the hard seat were marked. Since an exact match of the inter-ischial tuberosity distance was expected to be rare, we used a margin of error where the distance was no less than the measured minus 2mm and no greater than the measured plus 8mm. The margin of error was skewed to the larger side due to the fact that in a soft seat, the pressure mat is no longer a straight line between the ischial tuberosities, but has some curvature to it due to seat deformation. If a best-fit was found it was displayed on the image. If the estimate was reasonable the coordinates of the two points were saved to a file. There were several other possible scenarios that required further input:

1. No peak located in one of the outlined areas and one peak found in the other outlined area. In this case the single peak found on one side is assumed to be one ischial tuberosity and the area on the opposite side was manually searched for the most probable location of the highest pressure area, constrained by the arc that defines the inter-ischial tuberosity distance.
2. No peak located in one of the outlined areas and multiple peaks located in the other outlined area. In this case a best estimate of the correct peak was subjectively selected from the multiple peaks, and the opposite peak was determined as described above.
3. No peak located on either side. The user is forced to estimate the approximate location of one of the ischial tuberosities and then locate the opposite one constrained by the inter-ischial tuberosity distance for that subject.
4. Multiple peaks located on both sides but none meet the inter-ischial tuberosity distance requirement. This condition did not occur with our data. However, if it had, the user would have been forced to estimate one of the ischial tuberosities and then locate the opposite one the inter-ischial tuberosity distance for that subject.

Pressure Mat Image Quality

Image quality of the pressure mat data was subjectively evaluated to determine if pressure mat quality is affected by specific measurable variables such as hip breadth or subject sex. Pressure mat image quality was evaluated in a subjective manner on a scale from 0-5, with 0 being the lowest quality image and 5 the highest quality image based on the ease with which the ischial tuberosity pressure points could be discerned from the surrounding pressure data. We investigated the relationship between image quality and subject sex, and hip breadth.

3. Estimation of Pelvis Position through Multiple Measurements

In this report, we propose an approach to estimate the pelvis position of a driver using multiple measurements. We consider the pelvis to be a rigid object and determine its position by the anterior superior iliac spine (ASIS) point and the left and right ischial tuberosity (ISCH) points. We obtain multiple measurements of these three points from different positions of the driver. Then we develop a minimum variance estimator to estimate the 3D coordinates of the ASIS point and ISCH points based on the above multiple measurements.

The quantitative description of pelvis position is important for understanding driver posture, relating posture to comfort and therefore improving automobile seat design. As a rigid object, it is sufficient to determine pelvis position using three landmarks. In our approach, the right anterior superior iliac spine (ASIS) point and the left and right ischial tuberosity (ISCH) points are chosen. In general, these landmarks follow the recommendations by Cappozzo [31], which are

1. The relative movement between markers and underlying bone due to soft tissue deformation is minimum.
2. The distance between markers is sufficiently large.

We have also developed an efficient method for estimating the 3D coordinates of the above three landmarks on a subject in a natural driving position. A 3D data acquisition system based on stereoscopic perception is used to derive the 3D position of the right ASIS [30]. In Figure 1 we show a picture obtained by one of the cameras in our stereo system. The landmarks are outlined using dark curves.

The positions of the ISCH points are located using the pressure distribution system at the occupant-cushion surface [32]. The pressure measurement is obtained from a sensor mat which consists of 43x 48 pressure sensors, each sensor being 1 sq cm. A bivariate polynomial function is used to reconstruct the pressure distribution based on the scattered sensor data, as described above. The ISCH points are the peaks which are the local maxima in all directions. Figure 2 shows a pressure distribution on a seat surface and the peaks found by our approach.

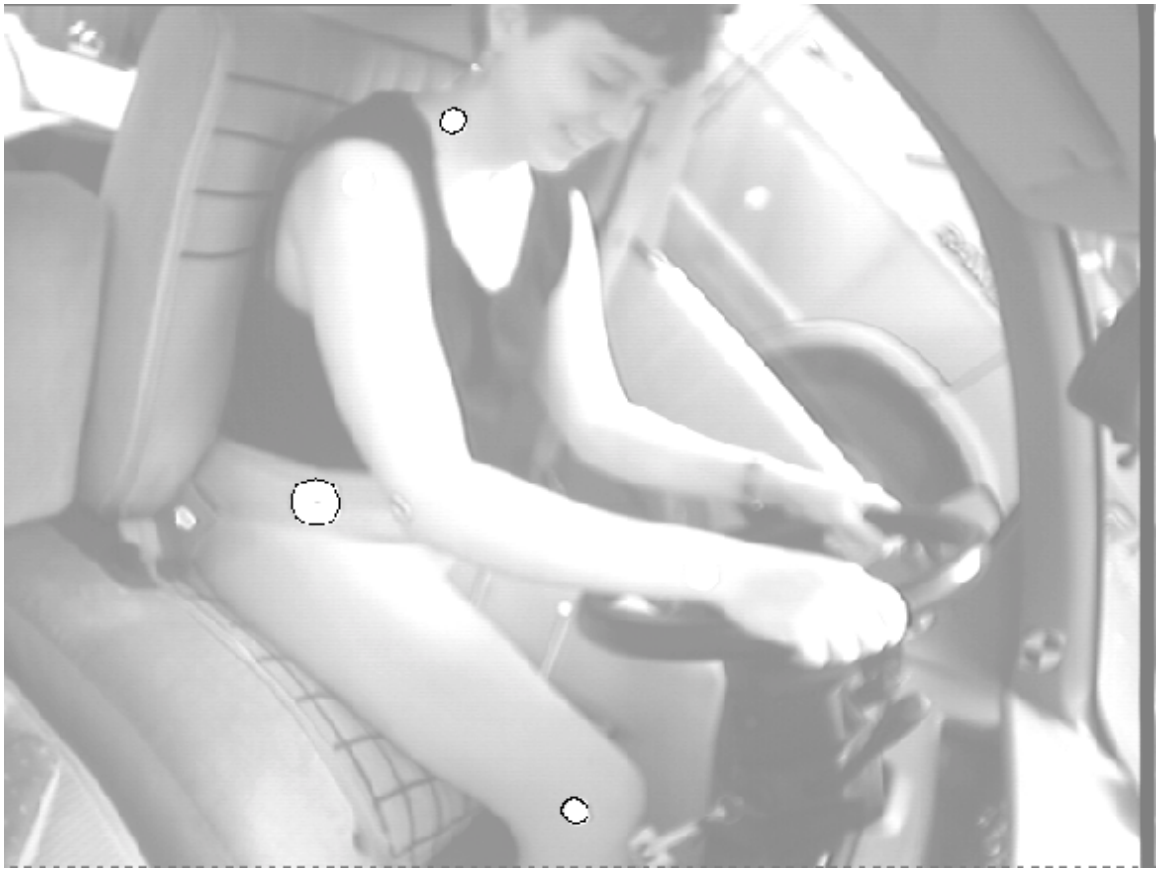

Figure 1 The landmarks are detected and outlined using dark curves (one of the targets is the right ASIS.)

However, these estimations are not perfect and suffer from various measurement errors. As we reported in [30], the errors of 3D coordinates obtained from our 3D data acquisition system is approximately 1 part per 500 or 0.2 percent of the field of view. These errors can come from various sources, such as camera calibration, lens distortion and stereo correspondence. The accuracy of the ISCH positions is limited by the sensor resolution. There are other factors such as presence of the tissue and clothing which will also affect the estimation.

There are two ways to improve the estimation of the pelvis position. One is to increase the number of external markers. This turns out to be very difficult. First, in order to create a natural driving environment, the measurement has to be non-invasive. Secondly, the visible portion of the pelvis of a driver is very limited because most of it is occluded by the seat and back cushion.

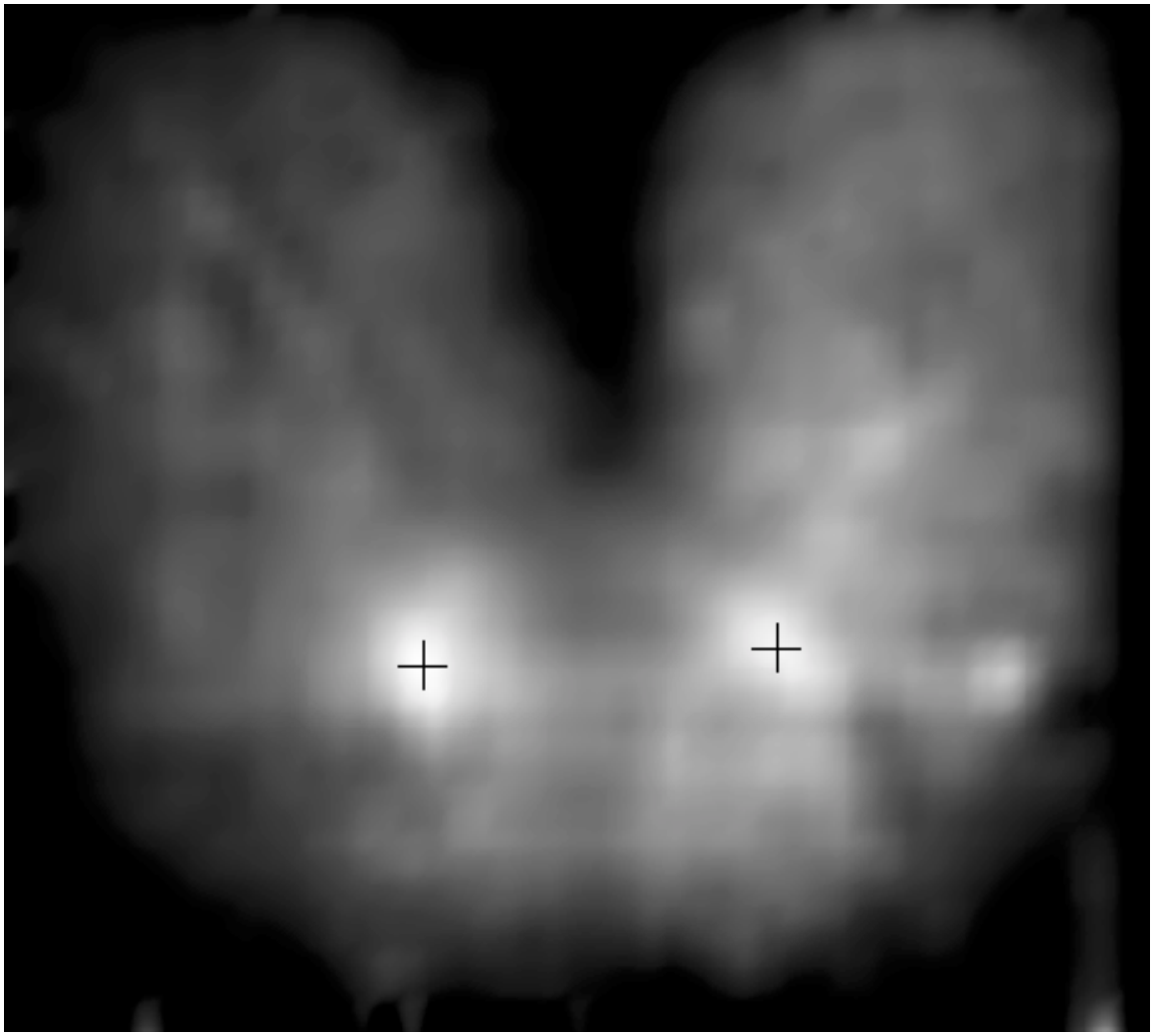

Figure 2 The pressure distribution at the occupant-cushion surface. The detected peaks are marked with dark crosses. The pressure value is proportional to the brightness.

An alternative method is to utilize redundant information from multiple measurements of the same object. In our driving experiments, each subject goes through a two-hour drive with video and pressure data collected at specific time intervals. This whole data set not only records the motion of the pelvis, but also provides the necessary information to improve our estimation. Besides the data from the drive, we also take the measurement of the subject's pelvis in the lab. In the lab, the right ASIS point is measured using a 3D electro-goniometer that is accurate to 0.3 mm and the ITCH points are found by a finer resolution pressure mat [33]. We also include the data from the lab to improve the estimation of pelvic position.

One of the key problems in many dynamic tasks is that of minimizing at a certain time a criterion that depends upon measurements that have been made previously, as well as upon some measurements that we are currently performing or will perform. For the sake of

efficiency, it is important to avoid going over the complete minimization process each time a new measurement is performed. It is also important to have an idea of how the next measurement will change the current estimate of the quantities with respect to those that we are minimizing. Those ideas are central to the theory of the Kalman filter [34].

The Kalman or extended Kalman filters are widely used in the problem of tracking an object in sequences of images or in sequences of stereo frames [35, 36, 37, 38]. In this report, we consider the pelvis as the object we want to track through multiple measurements, so similar Kalman filter techniques can be used. Unlike many computer vision problems, where the tracking is performed in a two-dimension to two-dimension fashion, if a monocular image sequence is used or a two-dimension to three-dimension if stereo frames are used, our problem is a three-dimension to three-dimension one.

In this report, we describe a minimum variance estimator to estimate the pelvis position through multiple measurements.

Dynamic Model

Assume we have *m* sets of measurement of a pelvis as shown in Fig. 3. For each measurement *i*, we obtain the three dimensional coordinates of the right ASIS point and two ISCH points. We denote the 3D coordinates of the right ASIS point, the right ISCH point and the left ISCH point at measurement *i* in a local coordinate system O_i as $\mathbf{X}_{i,1}$ $\mathbf{X}_{i,2}$ and $\mathbf{X}_{i,3}$ respectively. The transformation between different local coordinate systems *i* and *k* can be expressed using the following formula:

$$X_{i,j} = R_{i,k} X_{k,j} + T_{i,k} \qquad (6)$$

Our goal is to improve the estimation of the pelvis position based on the $\mathbf{X}_{i,j}$, where i=1,...,m and j=1,...,3 corresponds to each point on the pelvis. In the case of driving, it is reasonable to assume that a driver's pelvis undergoes a translation on the seat surface plane and a rotation along the line of the left and right ISCH points. This motion model is illustrated in Fig. 4 where *P* is the horizontal seat surface plane, *A* is the right ASIS point, *B* is the right ISCH point and *C* is the left ISCH point.

Reference position

We first define the *reference position* for a pelvis. Then, we transform each measurement to the coordinate system where the reference position is obtained through a rigid body motion.

The reference position is defined as shown in Figure 4 where the points A, B & C correspond to the ASIS, right and left ischial tuberosities, respectively. The origin is at the mid-point of the two ischial tuberosity points and the Y-axis is defined as the line from the right to the left ISCH point. The Z-axis lies on the plane defined by the three points A, B & C.

Next we show how to transform a measurement to the reference position coordinate system. Let the points *B* and *C* be the right and left ISCH points respectively, *A* be the right ASIS point, and *P* be the plane determined by the points *A*, *B* and *C* as shown in Fig. 4. Let $X_{i,j}$ be the *j*th point in *i*th measurement. The transformation has three steps. Firstly, we

rotate the pelvis along the *z* axis (with angle α) to make the line **BC** have the same direction as the *y* axis. Secondly, we rotate the pelvis along the *y* axis (with angle β) to make the plane determined by the right ASIS point and two ISCH points be vertical to the horizontal plane. Finally, we translate the pelvis to the origin of the reference position coordinate system. Let $\mathbf{X}_{r_{i,j}}$ be the reference position of *j*th point from the *i*th measurement. We have

$$X_{r_{i,j}} = \mathbf{R}_i X_{i,j} + T_i \qquad (7)$$

where $\mathbf{R}_i = \mathbf{R}_{\beta i} \mathbf{R}_{\alpha i}$ and

$$\mathbf{R}_{\beta i} = \begin{bmatrix} \cos\beta_i & 0 & \sin\beta_i \\ 0 & 1 & 0 \\ -\sin\beta_i & 0 & \cos\beta_i \end{bmatrix}$$

$$\mathbf{R}_{\alpha i} = \begin{bmatrix} \cos\alpha_i & -\sin\alpha_i & 0 \\ \sin\alpha_i & \cos\alpha_i & 0 \\ 0 & 0 & 1 \end{bmatrix}$$

in which α_i and β_i are the rotation angles along *z* and *y* axis respectively.

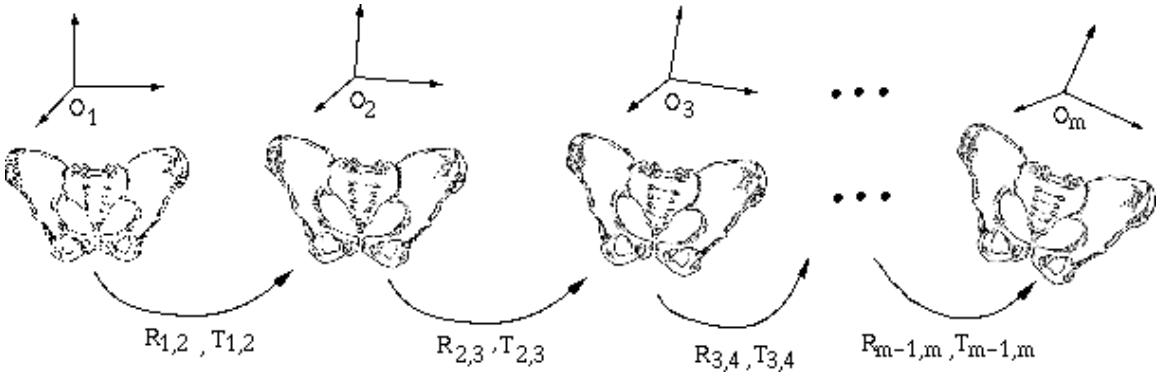

Figure 3 Multiple measurements of a pelvis. Each measurement is based on a local coordinate system. The transformation between local coordinate systems can be done using a rotation matrix and a translation vector.

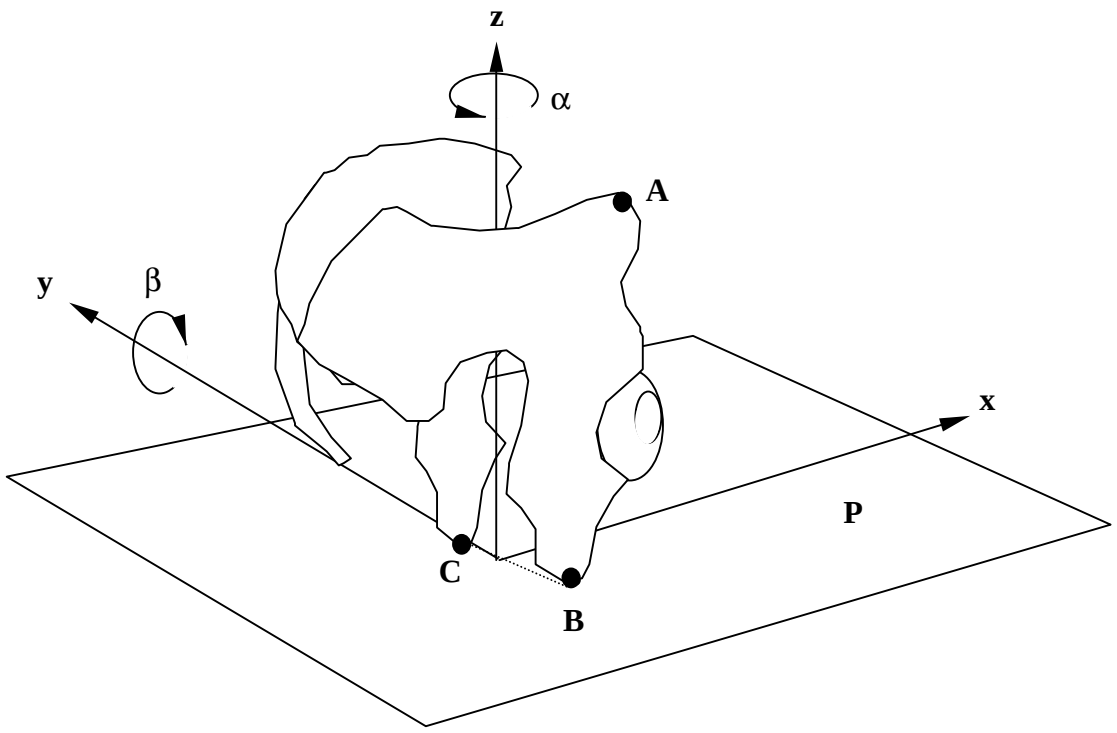

Figure 4 Reference position for the dynamic model. Origin is at the mid point between the two ischial tuberosities, z-axis lies on the plane defined by points A, B & C, with point A vertical to points B & C.

Minimum variance estimator

In this section, we present a minimum variance estimator to estimate the pelvis position from multiple measurements. Suppose that an observation vector y is related to a parameter vector m by an equation $y = Am + \delta_y$, where δ_y is a random vector with zero mean, $E(\delta_y) = 0$, and covariance matrix $\Gamma_y = E(\delta_y \delta_y^t)$. The unbiased, minimum variance estimator of m (i.e., that minimizes $E \| \bar{m} - m \|$) is the one that minimizes

$$(y - Am)^t (\Gamma_y)^{-1} (y - Am) \qquad (8)$$

(see, e.g. [39]). The resulting estimator is

$$\bar{m} = (A^t (\Gamma_y)^{-1} A)^{-1} A^t \Gamma_y^{-1} y \qquad (9)$$

where the error covariance matrix is estimated by

$$\Gamma_{\bar{m}} = \quad E(\bar{m} - m)(\bar{m} - m)^t \quad = \quad (A^t \Gamma_y^{-1} A)^{-1} \tag{10}$$

With a nonlinear problem, the observation equation becomes

$$y = f(m) + \delta_y \tag{11}$$

where $f(m)$ is a nonlinear function. As an extension from the linear model, we minimize

$$(y - f(m))^t (\Gamma_y)^{-1} (y - f(m)) \tag{12}$$

In other words, the optimal parameter vector m is the one that minimizes the matrix-weighted discrepancy between the computed observation $f(m)$ and the actual observation y. At the solution that minimizes equation(), the estimated $\bar{m}$ has a covariance matrix

$$\begin{aligned} \Gamma_{\bar{m}} = & \quad E(\bar{m} - m)(\bar{m} - m)^t \\ \cong & \quad \left\{ \frac{\partial f(\bar{m})}{\partial m} \Gamma_y^{-1} \frac{\partial f(\bar{m})}{\partial m} \right\}^{-1} \end{aligned} \tag{13}$$

One of the advantages of this minimum variance criterion is that we do not need to know the exact noise distribution, which is very difficult to obtain in most applications. The above discussion does not require knowledge of more than the second-order statistics of the noise distribution, which often, in practice, can be estimated.

Objective function

For each point j, we have the 3D coordinate X_{r_j} in the reference position coordinate system. Let $X_{r_{i,j}}$ be the 3D coordinate of point j in the reference position coordinate system based on ith measurement. According to the discussion in the previous subsection, we get the objective function for a minimum variance estimator as follows.

$$\min_{\forall X_{r_j}, \forall m} \sum_{i=1}^{N} \sum_{j=1}^{n} (X_{r_j} - X_{r_{i,j}})^t \Gamma^{-1}_{X_{r_{i,j}}} (X_{r_j} - X_{r_{i,j}}) \tag{14}$$

where N is the number of measurements, n is the number of points, and m is the collection of motion parameters (R_i, T_i) which transform the measurement in the local coordinate

system to the reference position coordinate system. The matrix $\left(\Gamma^{-1}_{X_{r_{i,j}}} \right)$ expresses the covariance for the *j*th point at the reference position from the *i*th measurement.

The above objective function (14) is neither linear nor quadratic, and an iterative algorithm is required to get a solution. The dimension of unknown parameters is large. Thus, a direct optimization is impractical. Our two procedures play a central role in resolving this problem.

First, a closed-form solution for motion between a local coordinate system and the reference position coordinate system is computed. Suppose we are given *N* corresponding points (p_i,p_i') which obey the relationship of

$$p_i' = Rp_i + T \tag{15}$$

The problem is: given equation (15), find *R* and *T*. The (p_i,p_i') are 3D coordinates of points on the surface of the rigid body in motion. It is well known that three noncollinear-point correspondences are necessary and sufficient to determine *R* and *T* uniquely.

Equation (15), when expanded represents three scalar equations in six unknown motion parameters. With three point correspondences, we will get nine nonlinear equations. Iterative methods can be used to obtain the `best' fits of the six unknowns. However, it is possible to get stuck in the local minima.

Blostein and Huang [40] use linear algorithms by observing that equation (15) is linear in components of *R* and *T*. Given four correspondences, $(p_i,p_i')_{i=1,2,3,4}$, we have the following linear equation:

$$\begin{bmatrix} p_{1x} & p_{1y} & p_{1z} & 1 \\ p_{2x} & p_{2y} & p_{2z} & 1 \\ p_{3x} & p_{3y} & p_{3z} & 1 \\ p_{4x} & p_{4y} & p_{4z} & 1 \end{bmatrix} \begin{bmatrix} r_{11} \\ r_{12} \\ r_{13} \\ t_1 \end{bmatrix} = \begin{bmatrix} p'_{1x} \\ p'_{2x} \\ p'_{3x} \\ p'_{4x} \end{bmatrix} \tag{16}$$

Similar equations can be obtained to solve (r_{21}, r_{22}, r_{23}, r_{31}, r_{32}, r_{33}, t_2 , t_3). The linear method uses four points instead of the minimum of three required for uniqueness. To overcome the problem of supplying the linear method with this extra point correspondence a `pseudo-correspondence' can be artificially constructed on the basis of rigidity of the body.

The second is to eliminate iteration on the structure. The gradient-based search is only applied to motions, because given each candidate set of motions, the best structure for equation (14) can be directly computed in a closed-form [41] by combining equations (7) & (14) to get:

$$X_{r_j} = \{\sum_{i=1}^{N} R_i \Gamma^{-1}_{X_{i,j}} R_i^t\}^{-1} \left\{\sum_{i=1}^{N} \{(R_i \Gamma^{-1}_{X_{i,j}} R_i^t)(R_i X_{i,j} + T_i)\}\right\} \tag{17}$$

The initial estimate for the reference position is obtained as follows. The three points for a given measurement ($\mathbf{X}_{i1}$, $\mathbf{X}_{i2}$, $\mathbf{X}_{i3}$) are rotated and translated (see equation (16)), until they correspond with the points A, B & C as illustrated in Figure 4. Thus, for each measurement position, an initial R_i and T_i can be estimated, with each measurement having three points A_i, B_i & C_i. Using equation (17), the initial reference position is obtained by using the initial estimates for R_i and T_i and the initial measurements $\mathbf{X}_{i,j}$ to determine ($\mathbf{X}_{r1}$,$\mathbf{X}_{r2}$,$\mathbf{X}_{r3}$), which correspond to the initial reference positions for the ASIS, right and left ischial tuberosities, respectively.

The initial reference position is used to determine a new set of rotation and translation matrices (R_i and T_i), by minimizing the objective function in equation (14), using a single step in a gradient-based search that holds ($\mathbf{X}_{r1}$,$\mathbf{X}_{r2}$,$\mathbf{X}_{r3}$) constant. The R_i and T_i are incrementally changed during the single iteration of the search solution for equation (14) and the new R_i and T_i are used in equation (17) to obtain a second reference position ($\mathbf{X}_{r1}$,$\mathbf{X}_{r2}$,$\mathbf{X}_{r3}$) estimate. The process is repeated ten times. The final R_i and T_i are applied to the final reference position for ($\mathbf{X}_{r1}$,$\mathbf{X}_{r2}$,$\mathbf{X}_{r3}$) to obtain the best estimate for the pelvis position for each pelvic measurement.

4. Comparing Pelvis Measurements to Design H-Point and D-Point Locations

Locating H-Point in the Seat Coordinate System. The design location of H-point for the 1995 Chevy Lumina was obtained from full scale drawings supplied by Delphi. In addition, one of the vehicle laboratories was evaluated using an H-point machine and Vectron at General Motors Corporation to measure the location of H-point.

The design coordinates for H-point are at (3140, 452) mm (X=horizontal and Z=vertical coordinates, respectively) using the SAE defined automobile coordinate system. The measured location of the H-point machine was at (3114, 452) mm. Thus the measured location was 26mm anterior to the design location of H-point. The differences are probably due to the extended track installed in the vehicle laboratories.

All position data collected in the vehicle laboratories are in a coordinate system based on the seat bolts and the seat track of the vehicle. The seat track has an incline of 7.5^o relative to the vehicle x-axis. The seat coordinate system used in this study was located so that the origin was at the top center of the right rear seat bolt. The X-coordinate was defined as positive parallel to the seat track in the anterior direction. The Y-coordinate was positive going from right to left (Figure 5) and the Z-coordinate was the cross product of X and Y.

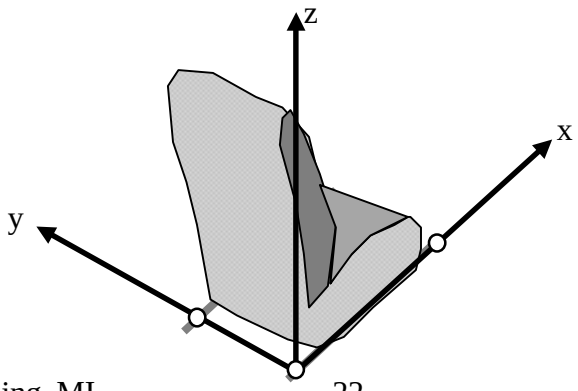

Figure 5 Seat Coordinate System.

Design drawings were used to determine the location of the seat bolt with respect to the car coordinate system. The top center of the bolt was located at (3098, 237) mm relative to the car coordinate system; thus, the position of the design H-point was 42mm behind the rear seat bolt and 215mm above it. The measured location of H-point was 17mm behind and 215mm above the rear seat bolt.

Converting H-point Location to the Seat Coordinate System. The seat coordinate system is defined with the X-axis positive from the rear bolt towards the front of the vehicle, while the SAE vehicle coordinate system is opposite. The H-point position is only reported with respect to the X-Z plane of the vehicle. The Y-coordinate is very sensitive to the dimensions of the subject, thus we did not evaluate the location of H-point with respect to the Y-axis.

The design and measured locations of H-point were expressed relative to the seat coordinate system by calculating the vector from the rear seat bolt to the respective H-point positions and rotating it by 7.5^{o}. The design H-point is at (-13.6, 218.6) mm and the measured H-point is at (11.2, 215.4) mm with respect to the seat coordinate system.

Comparing Subject Hip Joint to H-point Machine Measurement. The subject hip joint locations were determined as previously described. The seat positions were known for each video and pressure mat measurement, thus the measured location of the hip joint could be adjusted to the design position of the vehicle.

Fore/aft position corresponds to pure X-translation in the seat coordinate system. Rear riser height corresponds to a vertical translation along the Z-axis. The difference between the front riser and rear riser corresponds to the rotation of the seat pan about the rear riser. The distance from the origin of the seat coordinate system to the rear riser is 68mm posterior to the origin and the distance between front and rear risers are 250mm. The distance from the origin of the seat coordinate system to the top of the rear riser when the seat is in the rear-most and down position is 53mm (Figure 6).

The seat riser mechanisms have a complex movement pattern that can be simplified by the assumption that the position of the seat is independent of the sequence of riser adjustments and that the equivalent seat position can be achieved by raising both front and rear risers simultaneously followed by an adjustment of the front riser. Thus, we assume that the rotation is always about the rear riser.

We tested these assumptions and found that for a point at the center of the seat surface, errors between actual measurements and estimated position did not exceed 5.2mm for the entire range of seat motion. The greatest error occurred when both risers were at their highest position, and the smallest errors were when both risers were at their lowest positions. Further investigation revealed that these errors were caused primarily because the risers did not travel perpendicular to the track, but deviated from the perpendicular as a function of the height of the opposite riser. Instead of modeling this complex motion, we

elected to use the simpler model and accept that our average error would be between 0mm and 5mm. For any seat position where riser height was below half of the full height, the error was below 3mm. Since the majority of subjects did not raise the seat beyond half of the riser height, we feel using the simpler model is justifiable.

With the seat in the rear-most and most downward position, the rear seat riser is at the point (-67.4, 53) mm relative to the seat coordinate system. During the H-point machine measurement, the seat was moved forward 40mm and up 20mm relative to the rear-most and most inferior seat position with respect to the standard SAE vehicle coordinate system. To determine the seat position relative to the seat coordinate system, the vector (40, 20) was rotated 7.5^{o} resulting in the seat positioned at (42.2, 14.6) mm. Thus, during the H-point machine measurement, the top of the rear riser was located at:

Rear Riser = (42.2, 14.6) + (-67.4, 53) = (-25.2, 67.6) mm

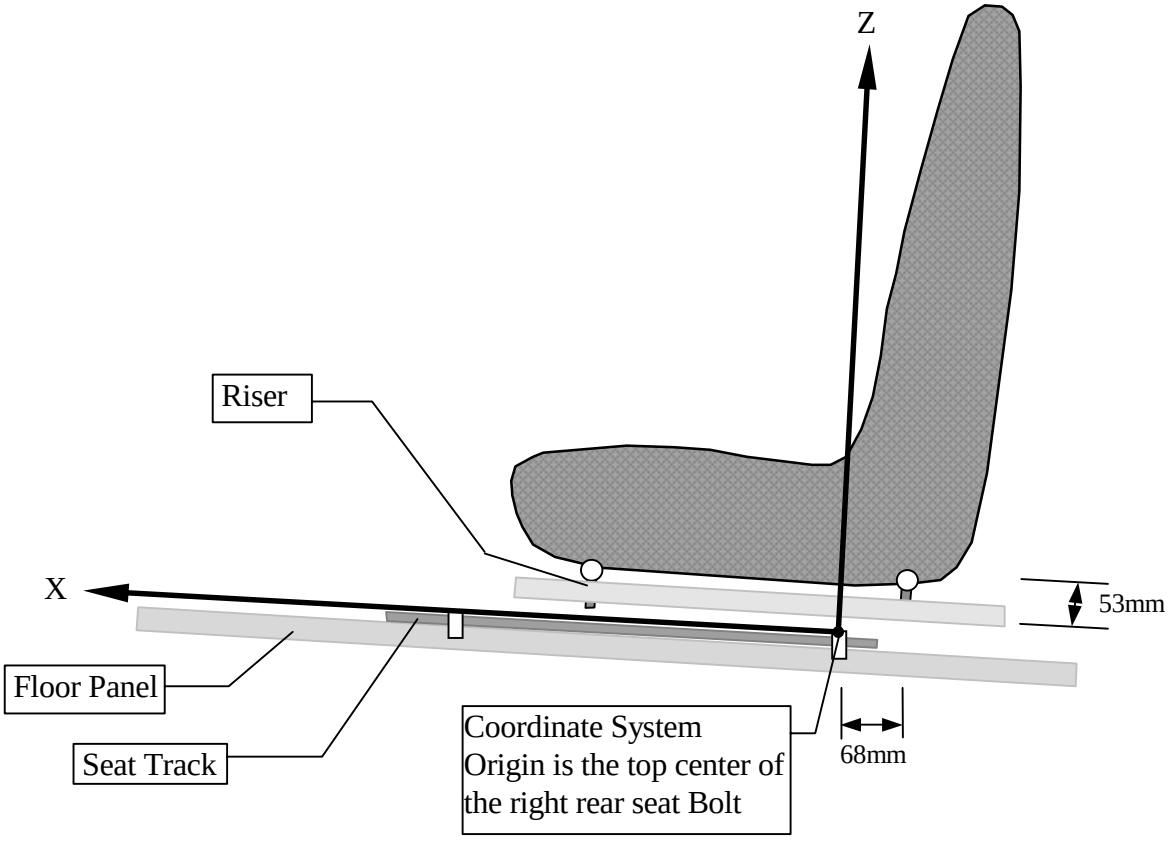

Figure 6 Relevant Seat Structures

The relationship between the H-point machine measurement of H-point and the location of a subject's hip joint is determined as follows:

1) Remove the effect of translation of the seat.

Let **R** be the position of the hip joint of a subject relative to the seat coordinate system. Let X_{RR} and Z_{RR} be the fore/aft position of the seat and the height of the rear riser, respectively and Z_{FR} be the front riser height. Then the point of interest on the seat is located at **r**, relative to the rear-riser in design position is:

$$\mathbf{r} = \mathbf{R} - (X_{RR} - 67.4, Z_{RR} + 53)$$

2) Remove the effect of rotation of the seat (i.e., the difference between front and rear riser height). The angle of the seat rotation is:

$$\theta = \text{atan}((Z_{FR} - Z_{RR})/250)$$

Rotating **r** into the seat position with both front and rear risers parallel:

$$\mathbf{r}' = [M(\theta)]\ \mathbf{r}$$

Where $[M(\theta)]$ is the rotation matrix required to rotate **r** by the angle θ and **r'** is the vector from the rear riser to the subject's hip joint if the front and rear risers were at equal heights.

3) Translate the vector **r'** to the seat located at the design measurement position. As stated, above, the rear riser was located at (-25.2, 67.6) during the H-point machine measurements. Thus, relative to the seat coordinate system, the subject's hip joint is at:

$$\mathbf{h} = \mathbf{r}' + (-25.2, 67.6)$$

Thus, comparing **H** = (11.2, 215.4) to the calculated value for **h** for each subject is one method for comparing the H-point machine measurement of H-point to the "user" location of their hip joint.

Locating D-Point. The design location for D-point is at (3172, 348) mm. The measured location of H-point was 25mm anterior to the design location. We assumed that the measured location of D-point can be determined by a simple translation of the design position; thus the measured location of D-point is assumed to be at (3147, 348) mm.

The origin of the seat coordinate system is at (3098, 237) mm; thus in the SAE car coordinate system, the vector from the rear seat bolt to D-point is (-49, 111). Converting this to seat coordinates, the measured location of D-point is at (-34.1, 116.4) mm. The

relationship between D-point and the location of a subject's ischial tuberosity is determined as follows:

1) Remove the effect of translation of the seat.

Let **D** be the position of the ischial tuberosity of a subject relative to the seat coordinate system. Let X_{RR} , Z_{RR} and Z_{FR} be as defined earlier. Then the point of interest on the seat is located at **d**, relative to the rear-riser:

$$\mathbf{d} = \mathbf{D} - (X_{RR} - 67.4, Z_{RR} + 53)$$

2) Remove the effect of rotation of the seat (ie the difference between front and rear riser height). The angle of the seat rotation is:

$$\theta = \text{atan}((Z_{FR} - Z_{RR})/250)$$

Rotating **d** into the seat position with both front and rear risers parallel:

$$\mathbf{d}' = [M(\theta)]\ \mathbf{d}$$

Where $[M(\theta)]$ is the rotation matrix described previously and **d'** is the vector from the rear riser pivot to the "users" ischial tuberosity location.

3) Translate the vector **d'** to the seat design position. As stated, above, the rear riser was located at (-25.2, 67.6) during the H-point machine measurements. Thus, relative to the seat coordinate system, the subject's ischial tuberosity is at:

$$\mathbf{d}'' = \mathbf{d}' + (-25.2, 67.6)$$

Locating the Eye. The design location for the X and Z datum intersection point of the eyellipse is at (3148, 1085) mm in the SAE car coordinate system. We used the design location of the eyellipse even though the H-point machine measured H-point as being 25mm forward of design, we assumed that the effect on the eyellipse is negligible.

The origin of the seat coordinate system is at (3097, 241) mm; thus a vector from the top of the rear seat bolt to the eyellipse is (-51, 844) mm in the SAE car coordinate system. Converting this to seat coordinates, the measured location of eyellipse is at (59.6, 843.4) mm. The relationship between the design position of eyellipse and the location of a subject's eye is determined as follows:

1) Remove the effect of translation of the seat.

Let **E** be the position of the eye of a subject relative to the seat coordinate system. Then the eye point, **e**, relative to the rear-riser is:

$$\mathbf{e} = \mathbf{E} - (X_{RR} - 67.4, Z_{RR} + 53)$$

2) Remove the effect of rotation of the seat (i.e., the difference between front and rear riser height). The angle of the seat rotation is:

$$\theta = \text{atan}((Z_{FR} - Z_{RR})/250)$$

Rotating **e** into the seat position with both front and rear risers parallel:

$$\mathbf{e}' = [M(\theta)]\ \mathbf{e}$$

Where $[M(\theta)]$ is the rotation matrix defined previously.

3) Translate the vector **e'** to the seat design position. As stated, above, the rear riser was located at (-25.2, 67.6) during the H-point machine measurements. Relative to the seat coordinate system, the subject's eye point is at:

$$\mathbf{e}'' = \mathbf{e}' + (-25.2, 67.6)$$

Thus, comparing **E** = (59.6, 843.4) mm to the calculated value for **e"** for each subject is one method for comparing the eyellipse to the "users" eye location.

5. Orientation of lap belt contact points on the pelvis.

Ideally the lap belt lies below the ASIS of the driver/occupant of any vehicle. If a person's posture is too slumped, then the chances for "submarining" (occupant sliding under the seat belt) increase in the event of an accident. There are two contact areas on the pelvis that can act to hold the lap belt to the pelvis. The first is the ASIS-AIIS line; the second is the ASIS-Notch angle (see Figure 7).

The orientation of these contact areas can be determined from existing pelvic data [42]. The pelvis orientation in this report will be described relative to the line from ASIS to the ischial tuberosity (Figure 7). Using the data on the ASIS, AIIS and the ASIS notch found in reference [42], the angle between the ASIS-ischial tuberosity line and the ASIS-AIIS line is -13.3^{o} while the angle between the ASIS-ischial tuberosity line and the ASIS notch is $+12.2^{o}$ (negative angle is counter-clock-wise). The orientation of these structures will be reported with respect to gravity (vertical line) for the modal position of the driver.

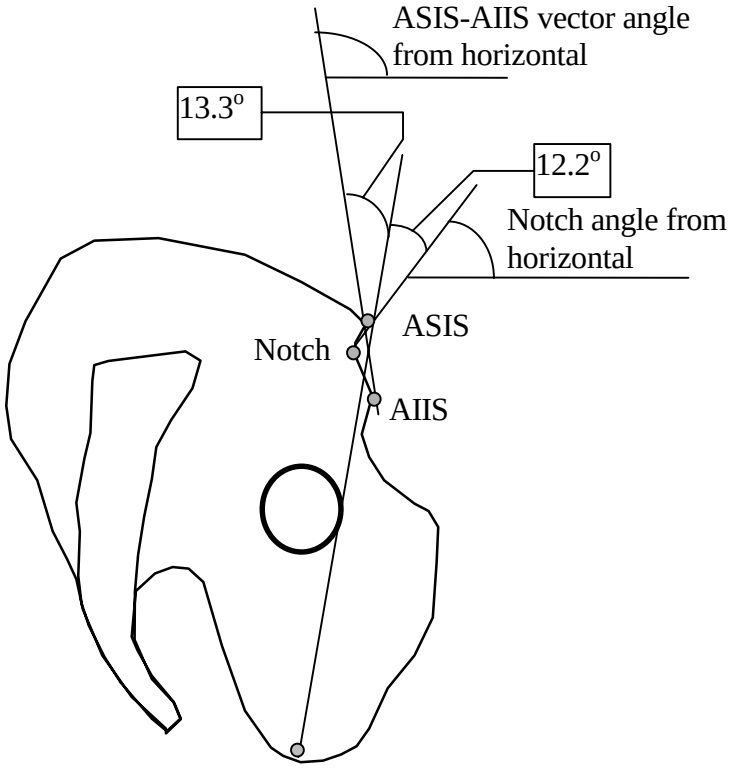

Figure 7 Angle of pelvic landmarks with respect to lap belt contact points.

6. Body Linkages and Joint Angles

The body was divided into linkages that are listed and defined in Table 1. Angles between the various linkages as well as angles relative to the coordinate axes are defined below. The definitions are summarized in Table 2 as well as illustrated in the figures below.

The neck angle was defined using two methods (Table 2 and Figure 8). The angle formed by the eye-neck target- hip joint was projected onto the XZ plane and defined the Neck1 angle. The angle formed by the eye-shoulder target-hip joint was projected onto the XZ plane to define the Neck2 angle.

The trunk angle was also determined using two methods (Table 2 and Figure 9). The angle between the Z-axis and the XZ projection of the line from the neck target to hip joint defined the Trunk1 angle. The angle between the Z-axis and the XZ projection of the line from the shoulder target to the hip joint defined the Trunk2 angle. The reason for examining two definitions for this angle was the need to investigate the stability of the shoulder joint for defining trunk orientation. The current Oscar design template uses the shoulder joint and hip joint to define trunk angle; however, the shoulder joint can move a great deal without any trunk motion occurring. Thus, in this report we will investigate the

relationship between shoulder joint and the shoulder-neck junction as means for defining trunk orientation. Both of these angles are reported as positive if the body is leaning backward, and negative if the body is leaning forward.

Linkage Name	**Linkage Definition**
Head1	Eye Point-Neck Target
Head2	Eye Point-Shoulder Target
Upper Arm	Shoulder Target-Elbow Target
Forearm	Elbow Target-Wrist Target
Trunk1	Neck Target-Hip Joint
Trunk2	Shoulder Target-Hip Joint
Thigh	Hip Joint-Knee Target
Shank	Knee Target-Ankle Target
Shoulder Link	Neck Target-Shoulder Target
Sternum	Suprasternale Target-Lower Sternum Target
Pelvis	ASIS Target-Ischial Tuberosity

Table 1 Definitions of body linkages from target and anatomical landmark measurements.

Joint/Angle Name	**Joint Angle Definition (Angle Between the following points/lines/linkages)**	**Figure**
Neck1 Angle	Eye-Neck-Hip (2D-XZ plane)	Figure 8
Neck2 Angle	Eye-Shoulder-Hip (2D-XZ plane)	Figure 8
Trunk1 Angle	Neck-Hip Line and Z axis (2D-XZ plane)	Figure 9
Trunk2 Angle	Shoulder-Hip Line and Z axis (2D-XZ plane)	Figure 9
Shoulder Y Slope (YZ)	Neck-Shoulder and Y axis (2D YZ plane)	Figure 10
Shoulder Y Slope (XY)	Neck-Shoulder and Y axis (2D XY plane)	Figure 11
Arm Angle from vertical	Shoulder-Elbow and Z axis (2D XZ plane)	Figure 10
Elbow Joint Angle (2D)	Shoulder-Elbow-Wrist (2D XZ plane)	Figure 10
Elbow Joint Angle (3D)	Shoulder-Elbow-Wrist (3D)	Figure 10
Hip1 Angle (2D)	Neck-Hip-Knee (2D XZ plane)	Figure 9
Hip2 Angle (2D)	Shoulder-Hip-Knee (2D XZ plane)	Figure 9
Hip2 Angle (3D)	Shoulder-Hip-Knee (3D)	Figure 9
Thigh Angle	Hip-Knee (2D XZ plane)	Figure 9
Knee Joint Angle (2D)	Hip-Knee-Ankle (2D XZ plane)	Figure 8
Knee Joint Angle (3D)	Hip-Knee-Ankle (3D)	Figure 8
Shoulder Angle	Elbow-Shoulder-Hip (3D)	Figure 11
Thigh Splay	Hip-Knee and X axis (2D XY plane)	Figure 11
Calf Angle	Knee-Ankle and X axis (2D XZ plane)	Figure 8
Calf Splay	Knee-Ankle and X axis (2D XY plane)	Figure 11

Table 2 Joint angle definitions.

The hip angle was also defined using two methods. The neck-hip joint-knee were projected onto the XZ plane with the angle between them defining Hip1 angle. The angle between the shoulder-hip joint-knee defined the Hip2 angle (Figure 9). The Hip2 angle was reported as a 3D angle as well as 2D (projecting the lines defining the angle onto the XZ plane).

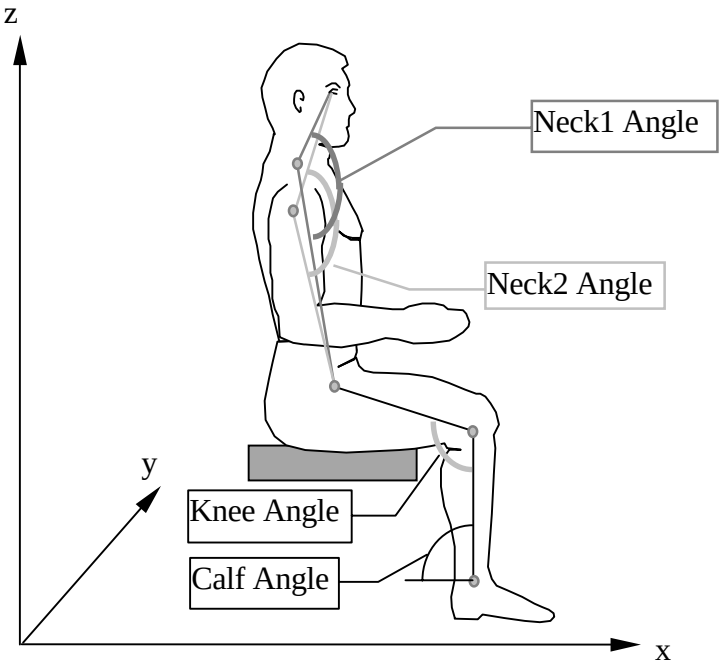

Figure 8 Neck Angle Knee Angle and Calf Angle definitions. All lines are projected onto the XZ Plane. The knee angle was reported as both a 2D and a 3D angle.

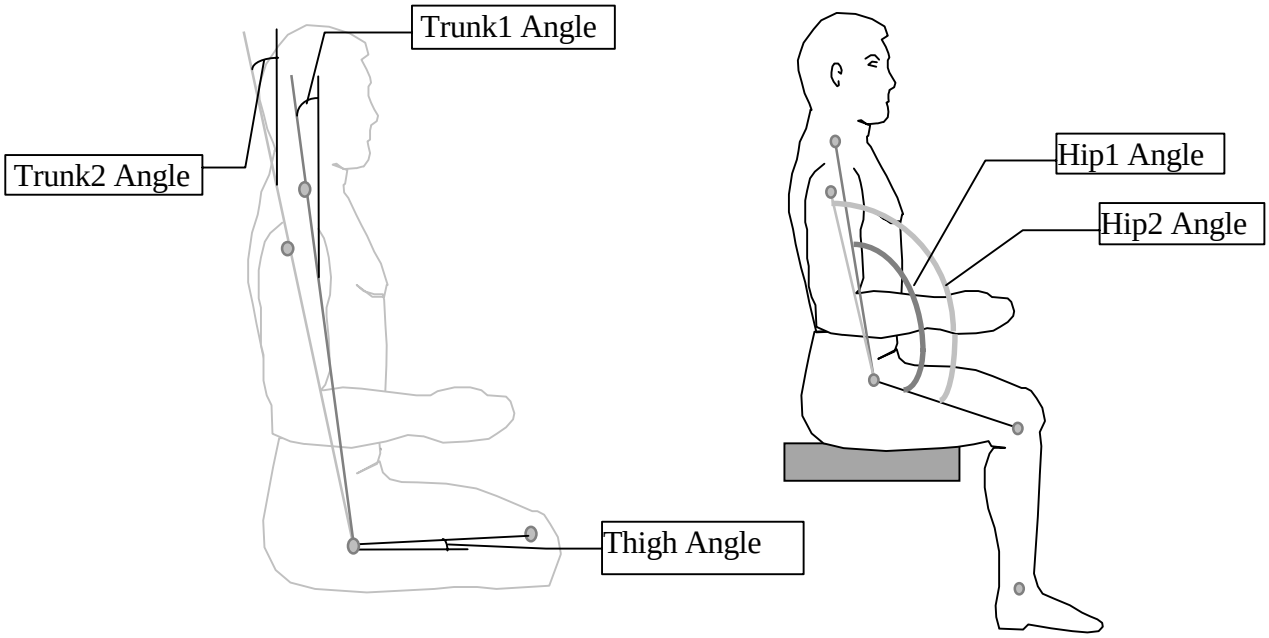

Figure 9 Trunk and Hip Angle definitions. All lines are projected onto the XZ plane.

The shoulder angle was defined as the angle between the elbow-shoulder-hip joint (Figure 11). The shoulder slope was described relative to both the YZ and the XY plane. The line from neck-shoulder targets was projected onto the YZ plane, with the angle from the Y axis defining the shoulder YZ-slope (Figure 10). The neck-shoulder line was projected onto the XY plane with the angle from the Y-axis defining the shoulder XY-slope (Figure 11).

The knee angle was defined using hip joint-knee-ankle targets. Both the 3D and 2D angles were calculated. For the 2D angle, the lines were projected onto the XZ plane and the angle between them defined the knee angle (Figure 8).

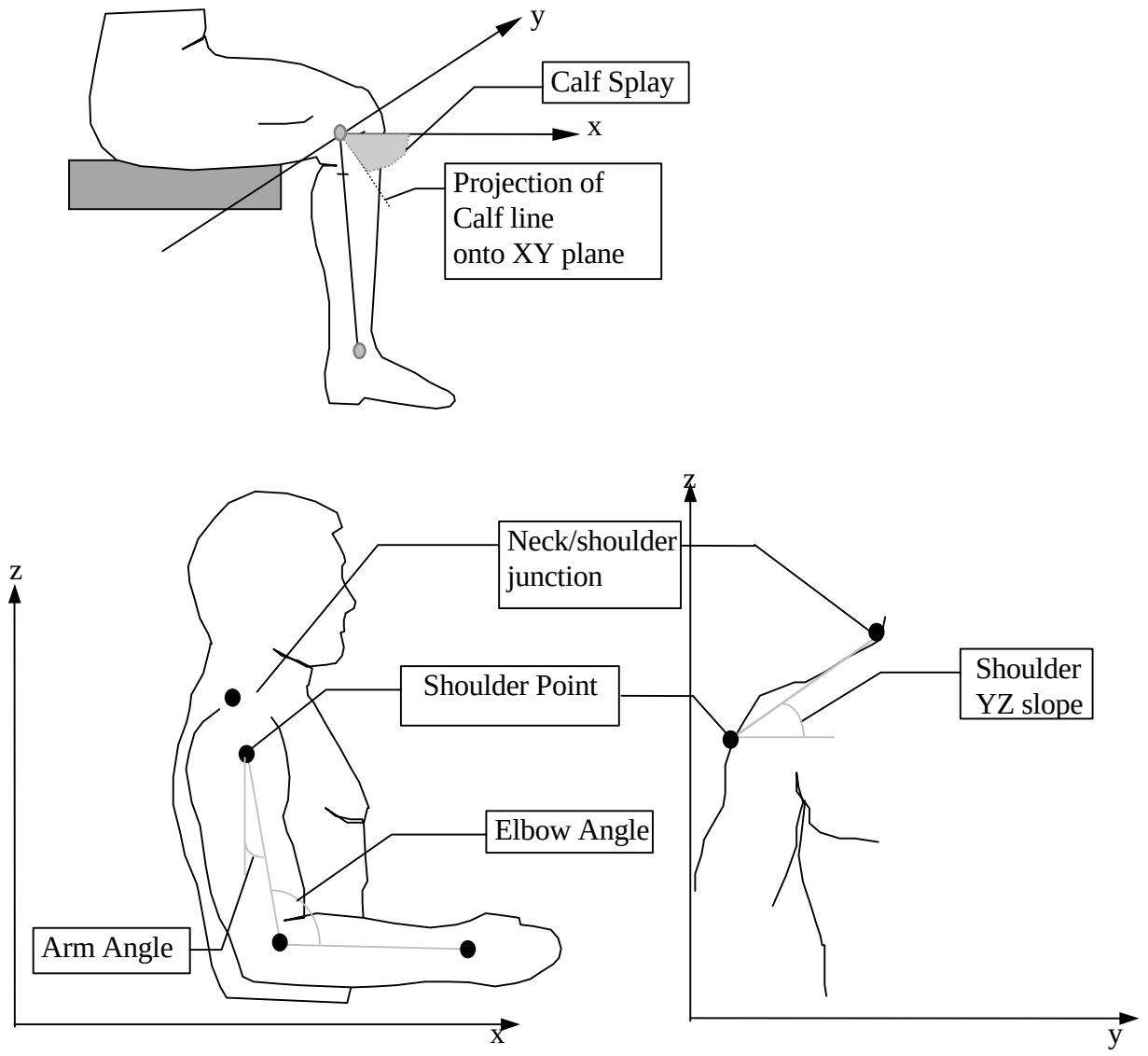

Figure 10 Calf Splay, Arm angle, Elbow angle and Shoulder YZ Slope definitions. All lines are projected onto the plane used to illustrate the angle.

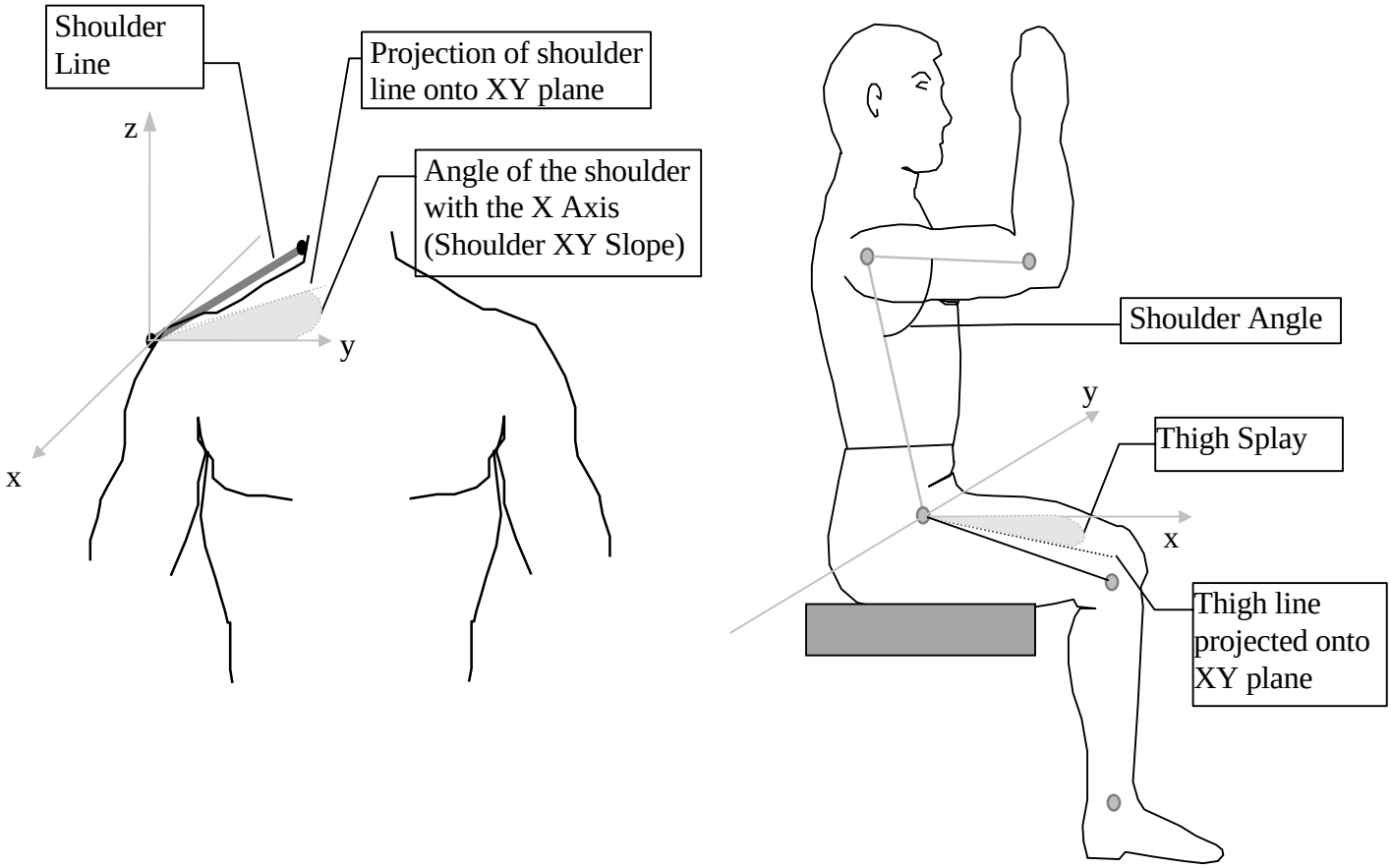

Figure 11 Shoulder XY-Slope, Shoulder Angle and Thigh Splay.

The 3D elbow angle was defined using the shoulder-elbow-wrist targets. The 2D elbow angle used the projection of the lines onto the XZ plane (Figure 11). The angle between the Z-axis and the shoulder-elbow line defined the arm angle (projected onto the XZ plane) (Figure 10).

The thigh angle was defined as the angle formed by the thigh link and the X-axis (projected onto the XZ plane) (Figure 9). This angle is positive if the knee is higher than the hip. Thigh splay angle was defined as the angle from hip joint-knee and the X-axis, projected onto the XY plane (Figure 11). The thigh splay angle is positive if the knee is further from the midline than the hip. Calf splay was defined similar to the thigh splay. The angle from the knee-ankle line and the X-axis, projected onto the XY plane, defined calf splay (Figure 10). The calf splay angle is positive if the ankle is closer to the midline than the knee.

7. Lumbar Spine Posture

In a previous report [43] we described a method for predicting the curvature of a subject's lumbar spine given the position of the chest relative to the pelvis. The lumbar curvature can be estimated using either the chest-pelvis angle as shown in Figure 12 or the distance from the X-position of suprasternale relative to the pelvic coordinate system

(Figure 12). The most accurate method for estimating a subject's lumbar curvature is to determine the regression equation between the chest-pelvis angle and the lumbar curvature or the regression equation between Suprasternale's X-position and lumbar curvature. Both methods provide similar estimates for the lumbar curvature, but the average of the two has been shown to be the most reliable [43]. Appendix A of reference [43] lists the regressions equations for all drive and lab subjects. Thus, in this report, the lumbar curvatures of drive subjects will be estimated using these regression equations.

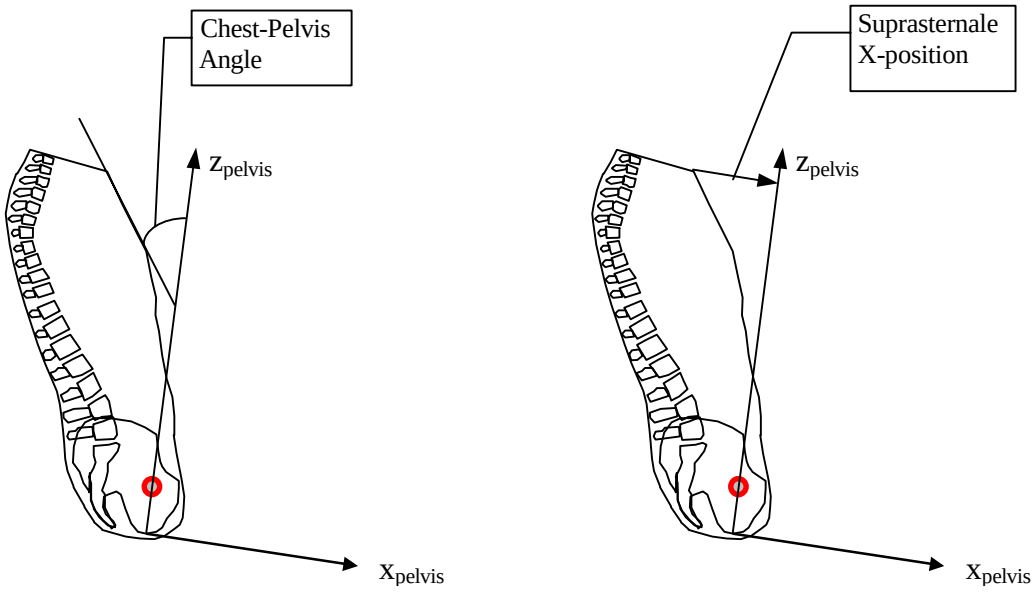

Figure 12 Pelvic coordinate system, chest angle, spinal height and spinal length.

III Results

A. Video Data Reduction

Target Visibility

In order for the three-dimensional position of a target to be determined it must be visible in at least two video camera images. In Table 3, the frequency with which targets were visible in any combination of cameras is listed. For example, the neck target was visible on cameras 1, 2 and 4 a total of 396 times out of a maximum of 448 images while it was only visible on the combination of cameras 1 and 2 a total of 4 times out of 448 images. The sternum2 target was not visible on any camera combination 293 out of 448 images (65%).

In Table 4 the frequency for which a target was visible by all combinations of two cameras are listed. From this data we can determine the camera pair best suited to viewing each target and the camera pair that provided the most data. For example, for the shoulder, cameras 1, 2 and 4 made the greatest contribution to locating the shoulder target while combinations with camera 3 made little contribution to locating that landmark.

	Not Visible on any camera	Camera 1,2	Camera 1,3	Camera 2,3	Camera 1,2,3	Camera 1,4	Camera 2,4	Camera 1,2,4	Camera 3,4	Camera 1,3,4	Camera 2,3,4	Camera 1,2,3,4
eye	86	4	1	37	3	4	82	37	17	3	138	36
neck	6	12	0	0	0	5	4	396	0	0	0	25
shoulder	7	4	0	0	1	10	3	291	0	0	0	132
sternum2	293	51	0	40	1	0	18	37	0	0	4	4
supra-sternale	176	56	0	86	6	0	32	74	0	0	13	5
elbow	31	0	0	18	0	0	75	0	78	0	236	10
wrist	7	3	0	27	0	0	47	175	0	1	94	94
RASIS	52	2	1	54	1	2	70	26	19	1	153	67
knee	15	0	0	20	0	0	59	12	30	0	243	69
ankle	237	0	3	1	0	11	0	0	187	9	0	0

Table 3 Frequency targets were visible for all camera combinations. There were a total of 448 video anthropometry images.

Error Analysis

In this section we describe the errors of the video anthropometric system. The absolute (Euclidean) error in locating the 3-D position of 69 known landmarks is summarized in the frequency distribution shown in Figure 13. The absolute error is usually less than 3mm, but the error can be as large as 5.5mm.

The effects of different individuals using the 3DAQ software to locate targets were also examined. Three individuals examined the same set of images for one subject. The average link length and standard deviation of the link lengths are given in Table 5 for each of the three examiners. In addition, the average and standard deviation of each link length is given for all three examiners. The smallest standard deviations were for the Suprasternale-

sternum targets, while the largest differences between examiners occurred at the RASIS-knee and Suprasternale-RASIS targets.

	Cameras 1&2 (%)	Cameras 1&3 (%)	Cameras 1&4 (%)	Cameras 2&3 (%)	Cameras 2&4 (%)	Cameras 3&4 (%)
eye	17.9	9.6	17.9	47.8	65.4	43.3
neck	96.7	5.6	95.1	5.6	94.9	5.6
shoulder	95.5	29.7	96.7	29.7	95.1	29.5
sternum2	20.8	1.1	9.2	10.9	14.1	1.8
Suprasternale	31.5	2.5	17.6	24.6	27.7	4.0
elbow	2.2	2.2	2.2	58.9	71.7	72.3
wrist	60.7	21.2	60.3	48.0	91.5	42.2
RASIS	21.4	15.6	21.4	61.4	70.5	53.6
knee	18.1	15.4	18.1	74.1	85.5	76.3
ankle	0.0	2.7	4.5	0.2	0.0	43.8

Table 4 Frequency targets were visible in each camera pair. As a percent of the total of 448 video anthropometry images.

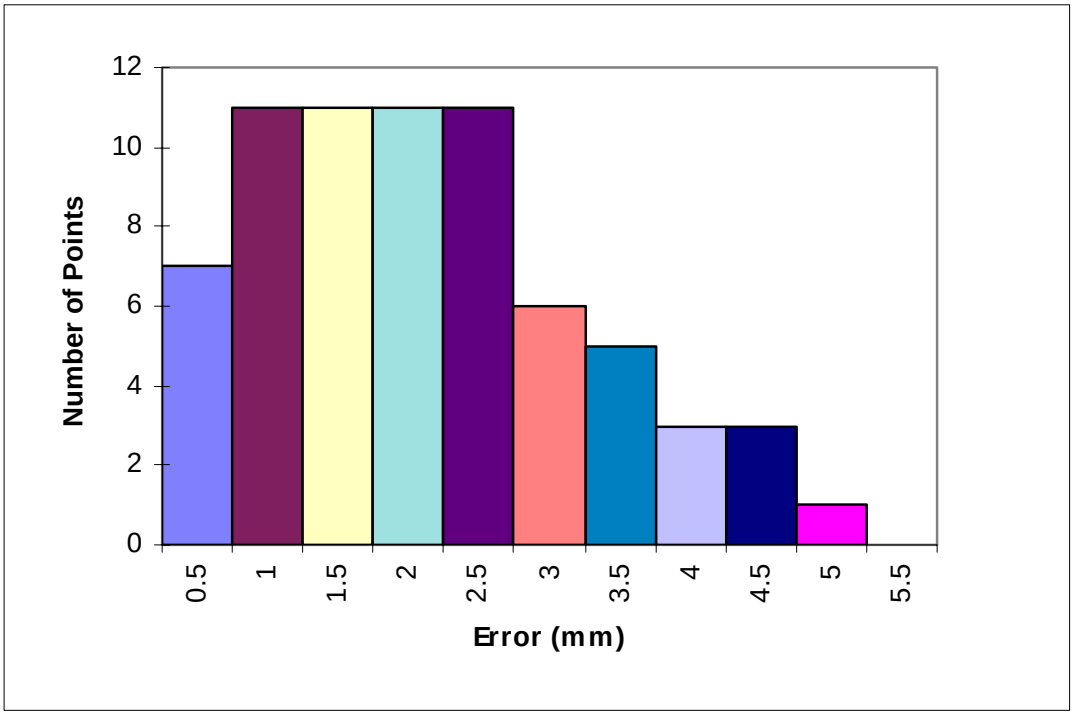

Figure 13 Measurement errors of the video anthropometry system.

Individual Examiner		Knee - Ankle	Acrom.- Elbow	Elbow- Wrist	S.Strn- Strnm	RASIS- Knee	S.Strn- RASIS	S.Strn - Neck	Door - Wheel	Wheel- A-pillar
A	**Mean**	421.10	272.94	255.00	42.63	392.66	314.16	143.14	390.79	248.26
	St Dev.	4.69	2.05	2.28	2.70	13.39	19.41	2.54	12.56	3.21
B	**Mean**	NA	272.73	255.28	42.49	390.21	313.86	142.24	387.78	250.88
	St Dev.	NA	2.36	2.43	1.15	12.11	18.24	2.87	7.11	1.90
C	**Mean**	415.60	272.99	255.19	41.73	390.64	314.97	142.17	NA	NA
	St Dev.	6.38	2.98	2.44	1.00	12.47	18.89	0.97	NA	NA
A,B,C	**Mean**	417.85	273.02	255.11	42.28	390.42	314.33	142.51	388.98	249.76
	St Dev.	5.29	2.37	2.19	1.61	11.83	16.33	2.03	8.21	2.68

Table 5 Link length comparisons for three individuals using the 3DAQ software to measure the same targets on the image sets for one subject.

The errors for individual subjects were estimated by comparing the link lengths for the drive images of every subject. For example, during the free drive a subject may have six sets of video anthropometry images recorded. The link lengths were averaged and the absolute difference between each link length measurement and the average was used as an estimate of the measurement error. The absolute error estimates for each link length were then averaged to provide an estimate of the error associated with a given image set. The frequency of errors was then determined (Figure 14). There were a total of 454 image sets, with 82.8% of the error estimates less than 5mm (Table 6).

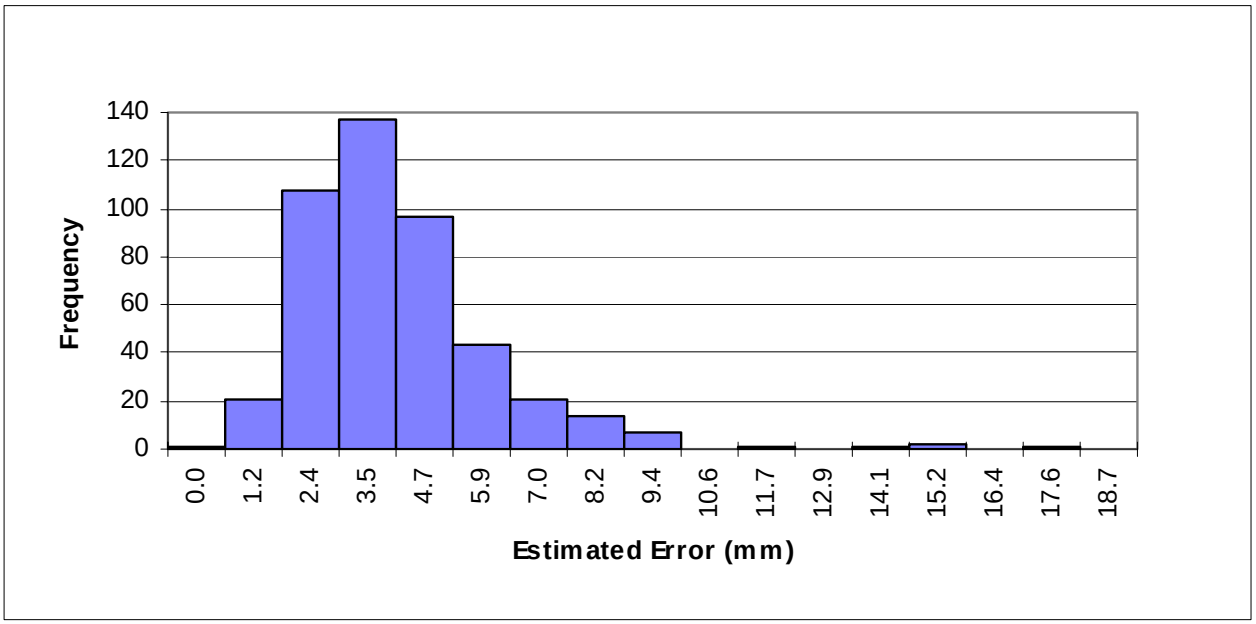

Figure 14 Frequency of errors using average link length as an estimate of true link length.

The average absolute errors are given for body segments as well as vehicle landmarks in Table 7. The largest error estimates are for the RASIS-knee link length, which has an average absolute error of 6.7mm, with 20.2% of the image sets having differences greater than 10mm. The fact that this is not a rigid link explains part of this large error. However, most of the errors were small, with the Suprasternale-sternum link having an average absolute error of 1.5mm and 100% of the image sets having error estimates of less than 10mm.

Error Level	Number of Measurements in Error Category (N =454)	Percent
Err < 5mm	376	82.8
Err < 7mm	427	94.1
Err <10mm	448	98.7
Err >10mm	6	1.3

Table 6 Error estimates from 454 video anthropometric measurements.

	Knee - Ankle	Shldr-Elbow	Elbow-Wrist	S.Strn-Sternum	RASIS - Knee	S.Strn-RASIS	S.Strn-Neck	Door - Wheel	Wheel - Apillar
Ave Abs Err (mm)	3.6	2.5	2.7	1.5	6.7	5.9	2.6	2.7	1.8
St Dev (mm)	4.2	3.5	2.3	1.3	5.7	5.4	3.9	2.2	1.4
Count	209	420	421	146	397	135	146	80	114
%Err < 5mm	78.0%	90.7%	87.6%	97.9%	45.8%	53.3%	88.4%	85.0%	97.4%
%Err < 7mm	88.0%	96.0%	96.0%	99.3%	62.2%	71.9%	94.5%	95.0%	99.1%
%Err <10mm	93.8%	98.3%	99.3%	100.0%	79.8%	85.2%	95.9%	98.8%	100.0%
%Err >10mm	6.2%	1.7%	0.7%	0.0%	20.2%	14.8%	4.1%	1.3%	0.0%

Table 7 Summary of error estimates for body segments and fixed car landmarks.

B. Pressure Mat Analysis and Pelvis Location

In this section we describe the analysis of pressure mat data and the location of the pelvis relative to the car seat. For the pressure mat data we will describe the quality of the pressure data regarding the ability to determine the location of the ischial tuberosities. The quality was rated on a 5 point scale with 0 being poor and 5 high quality (for locating peak pressure under the ischial tuberosities). The results are summarized in Table 8. This subjective analysis reveals that it was easier to determine the ischial tuberosity points on males (p=.005). We speculated that hip-breadth may be a factor and analyzed the regression of pressure mat image quality versus hip-breadth. The $r^2 = 0.12$, indicating that hip-breadth is only weakly correlated to pressure mat image quality.

There are three variables we will describe regarding the location of the pelvis: the hip joint location of subjects compared to H-point; the ischial tuberosity location compared to D-point and the angle of the pelvis relative to the Z-axis of the camera coordinate system. The H-point window is illustrated in Figure 15. This is the area the H-point will occupy if the seat is moved throughout the range of seat motion and H-point stays in a constant

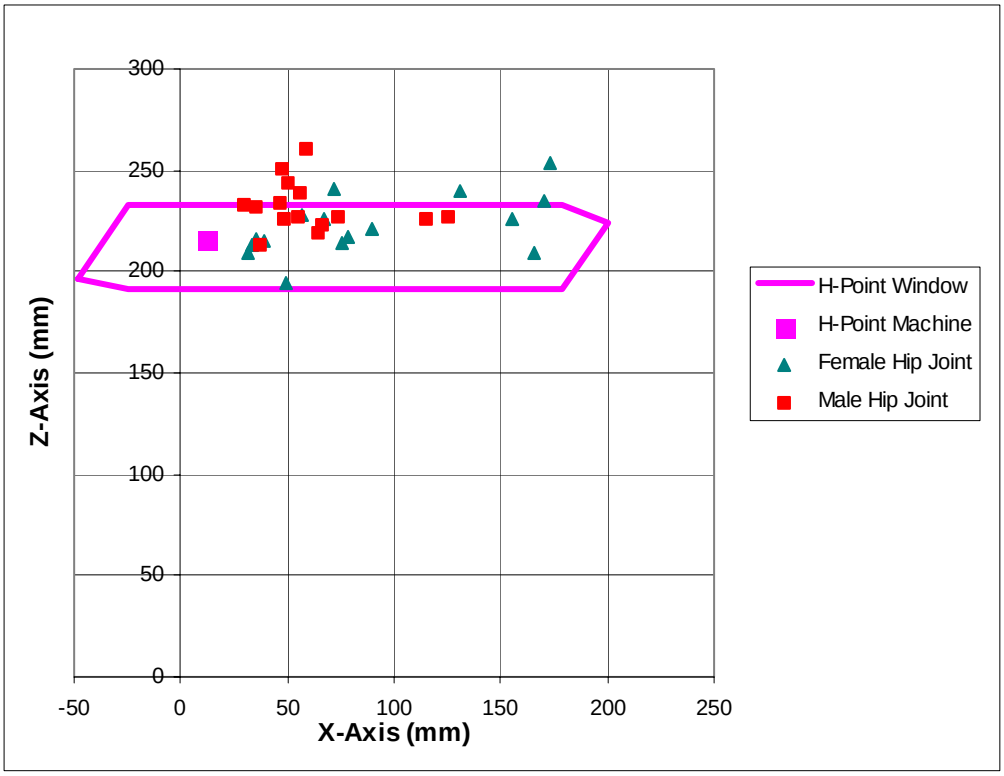

Figure 15 Hip joint locations relative to the H-point Window. Data is for the beginning of the modal period of the free drive.

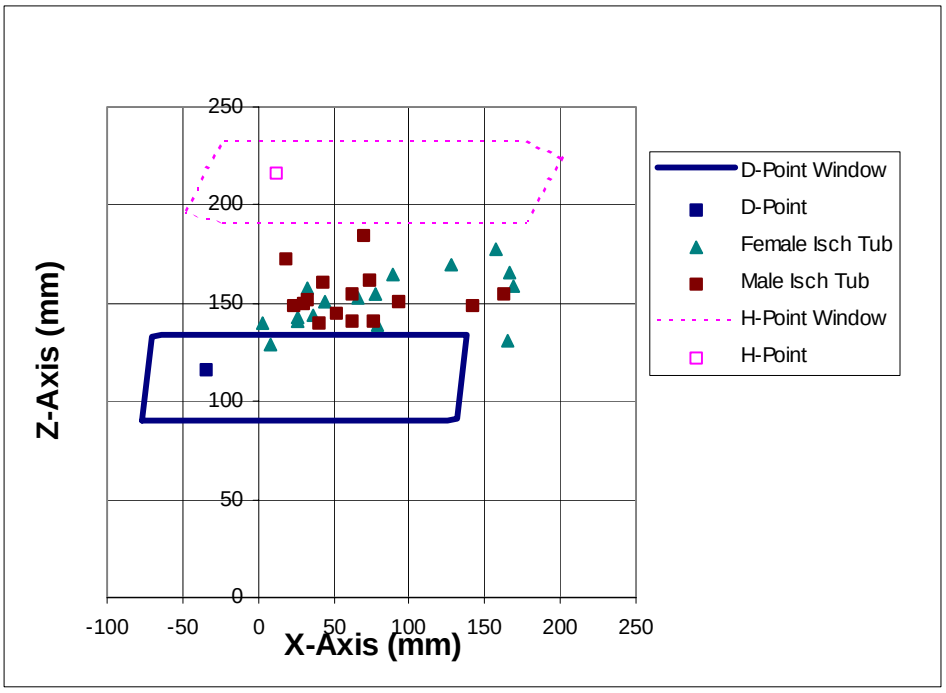

Figure 16 Ischial tuberosity locations compared to the D-point window. Data is for the beginning of the modal period of the free drive.

position relative to the seat. The measured position of H-point from the H-point machine is also illustrated in Figure 15 along with the male and female hip joint locations at the beginning of the subject's modal position.

The travel of D-point (D-point window) is illustrated in Figure 16; the design position of D-point (adjusted for the extended track) is also illustrated in the same figure. The locations of the ischial tuberosities are shown for males and females. For comparison, the H-point window and the location of H-point as measured by the H-point machine are also illustrated.

The data in the previous two figures are not adjusted for seat position. The H-point and D-point information are all given relative to the camera coordinate system (which is the same as the seat coordinate system). In the following two figures we correct for seat position so that the subject's pelvis measurements are translated and rotated to the position the seat was placed for the H-point machine test. This provides a means for comparing the location of H-point and D-point to the subject's hip joint and ischial tuberosity, respectively. Figure 17 illustrates the position of H-point as measured with the H-point machine compared to the position of each subject's hip joint. The data in Figure 17 are for the beginning of the modal period.

In Figure 18 the position of D-point is compared to the subjects' ischial tuberosity location. The data in Figure 18 are for the beginning of the modal period. The subjects' hip joint and ischial tuberosity positions were mapped back to the design position of the seat using the methods described in Section II of this report.

	P-Mat Image Quality	Hip Breadth
F Ave	2.4	39.9
F Std	1.3	2.4
M Ave	3.4	37.7
M Std	0.9	3.1

Table 8 Average pressure mat quality and hip breadth for males and females.

	Hip Joint Beginning		Hip Joint End		Isch Tub Beginning		Isch Tub End	
	X	Z	X	Z	X	Z	X	Z
F ave	87.4	219.2	86.9	219.3	79.5	148.2	79.3	148.7
F Stdev	22.0	22.4	15.7	21.8	31.4	22.6	26.9	21.7
M Ave	85.2	231.8	81.7	234.2	90.4	153.6	86.3	146.9
M Stdev	26.9	16.3	31.9	13.9	43.1	17.4	46.4	43.1
	Measured H-Point				Measured D-Point			
	X		Z		X		Z	
	11.2		215.4		-34.1		116.4	

Table 9 Hip joint and ischial tuberosity average location and standard deviation for the beginning and end of the modal position.

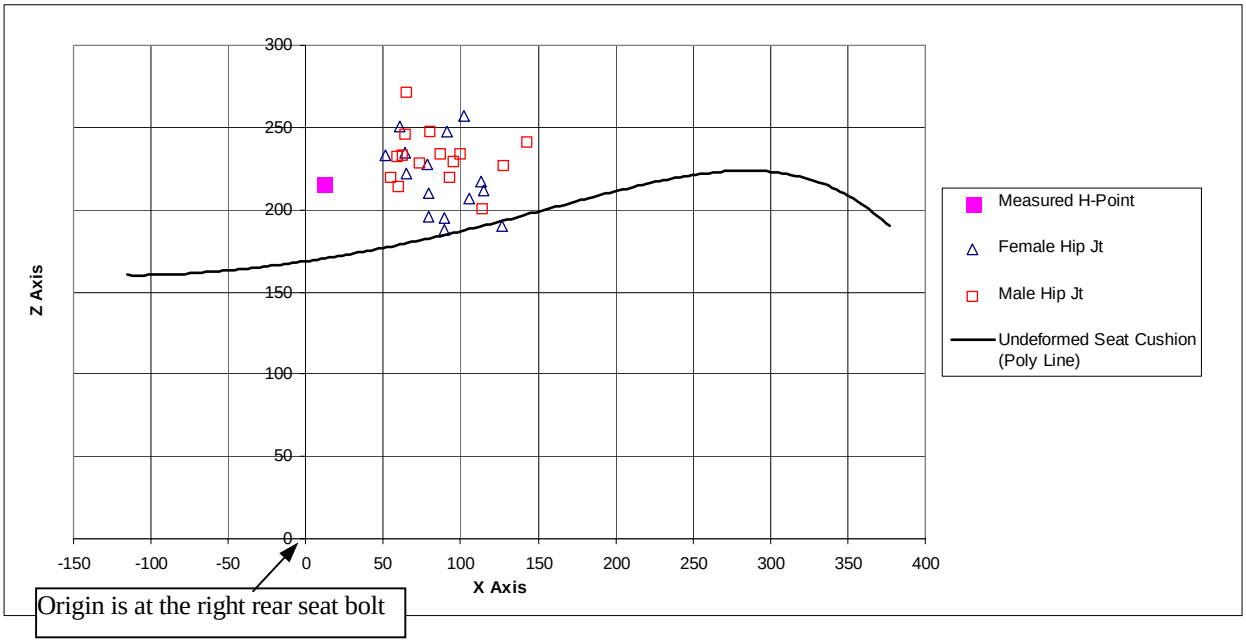

Figure 17 H-point compared to subject hip joint locations, adjusted for seat position at the beginning of the modal period in the free driver.

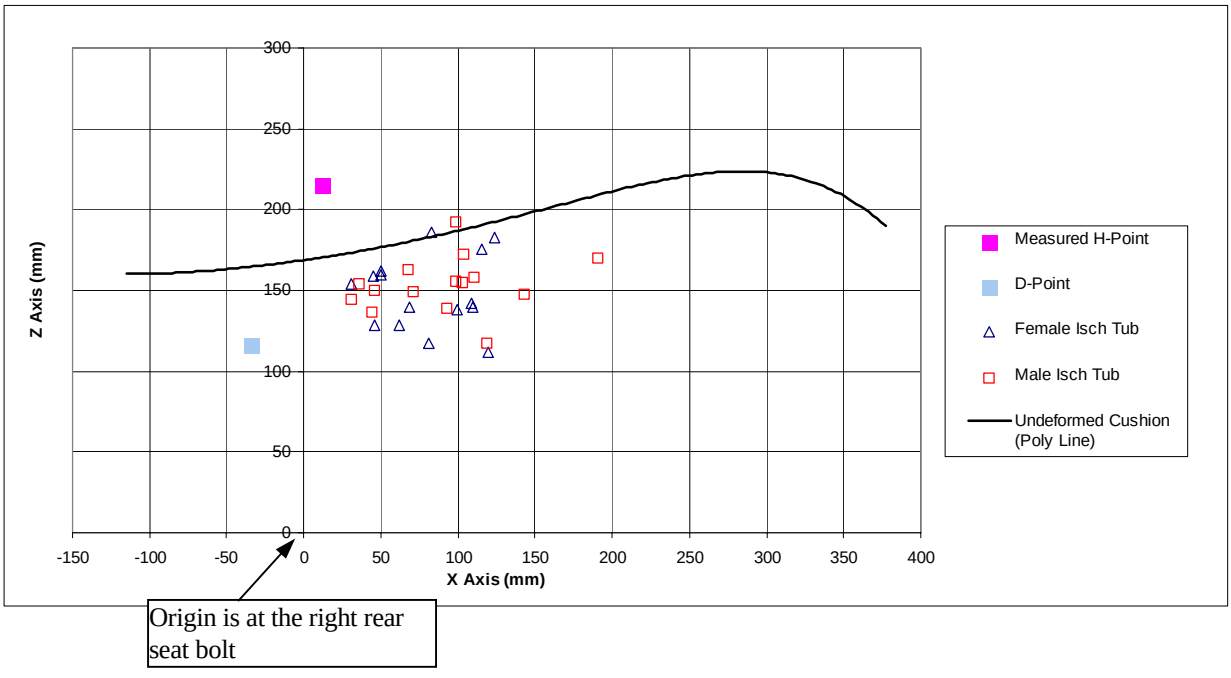

Figure 18 D-point compared to subject ischial tuberosity locations, adjusted for seat position at the beginning of the modal period of the free drive.

In Figure 19 the average hip joint and ischial tuberosity locations for males and females are compared with the measured H-point and D-point. The center line contour of the seat is also illustrated in the figure to provide a physical reference to the seat.

The average location of male and female hip joint centers and ischial tuberosity locations are summarized in Table 9 for both the beginning and end of the modal position. Table 9 includes standard deviations as well as the measured position of H-point and D-point.

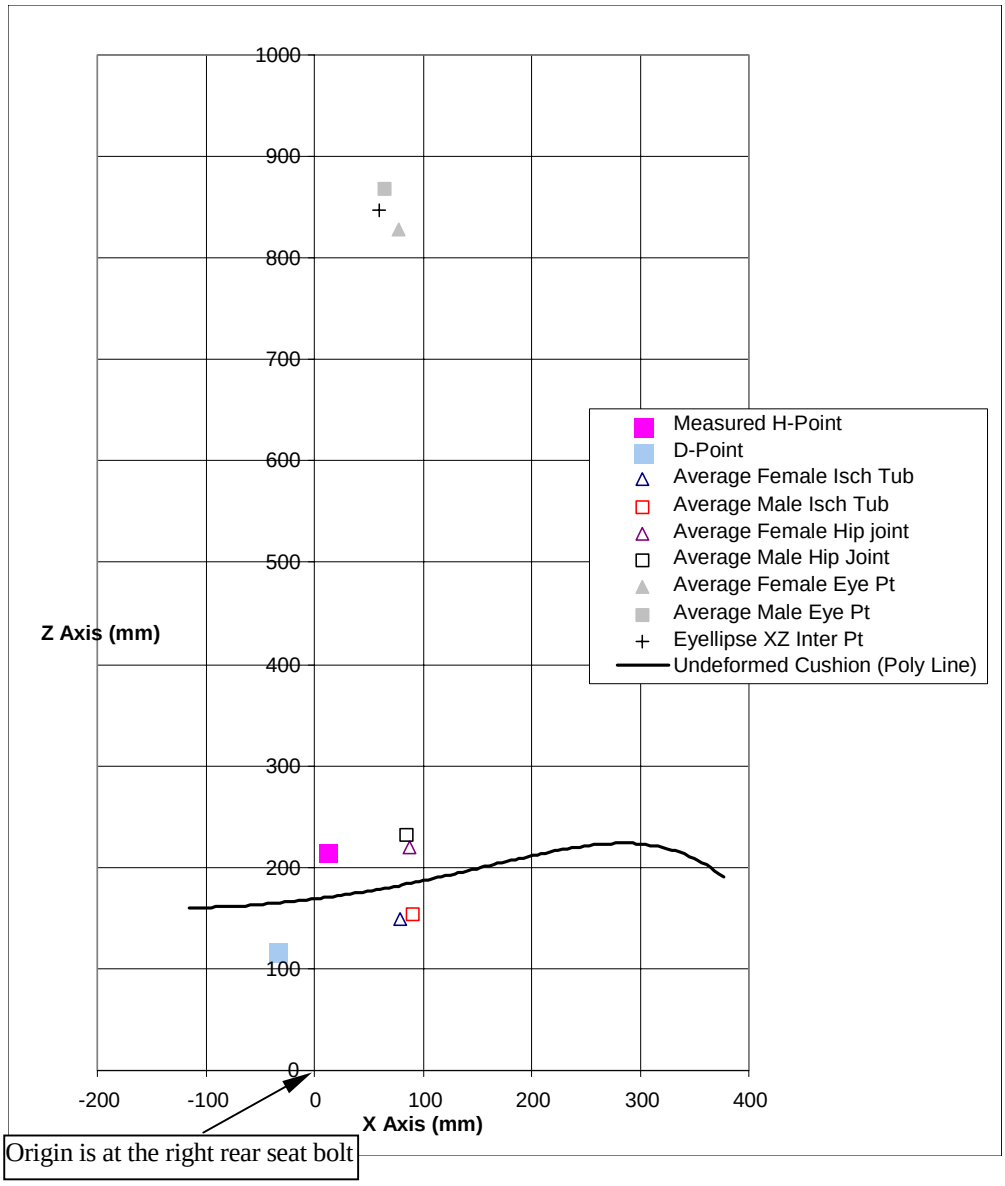

Figure 19 Average hip joint and ischial tuberosity locations compared to H-point and D-point at the beginning of the modal period of the free drive. The average eye points are also illustrated for males and females, with the XZ intersection of the eyellipse shown for reference.

A line from the ASIS to the ischial tuberosity defines the pelvis angle. The angles are relative to the camera coordinate system and were adjusted for seat pan tilt. The pelvis angles for males and females are illustrated in Figure 20, showing the distribution of pelvic angles at the beginning and end of the modal period of the free drive. There is a significant difference between males and females with regard to the pelvic angle ($p < 0.04$) for both the beginning and end of the modal period. On average, females had their pelvis tilted further forward than males, with an average of 12.9^o compared to the male average of -2.1^o at the beginning of the modal period (Table 10). The lumbar curvature is discussed in the next section.

The pelvic angles were examined with respect to the comfort classification of each subject at the beginning and end of their modal period (CC, UU and CU/UC). The CC subjects are clustered near a zero pelvic angle while UU subjects have their pelves tilted further forward and CU/UC subjects have their pelvis angle spread between erect and slumped postures (Figure 21).

	Pelvis Angle (corrected for seat pan tilt)		**Pelvis Angle (not corrected for seat pan tilt)**		**Lumbar Curvature**	
	Ave (deg)	**Std (deg)**	**Ave (deg)**	**Std (deg)**	**Ave (rad/SH)**	**Std (rad/SH)**
Beginning F	12.9	16.8	11.5	14.5	-0.29	0.64
Beginning M	-2.1	17.3	-1.6	16.2	0.20	0.95
End F	13.4	15.9	11.8	13.2	-0.43	0.54
End M	-5.3	19.4	-2.7	17.9	0.08	0.92

Table 10 Pelvis angle and lumbar curvature at the beginning and end of the modal period.

During the free drive, subjects changed their pelvis position at least 130 times (out of 40 drivers), for an average of 3.25 pelvis position changes during the drive. This estimate is low, since there were several times during the drive when either pressure data or video data was not available to measure the pelvis. Out of the 130 measurements, the average change in pelvis angle was $4.7^o \pm 2.4^o$ and the range of pelvis angles (minimum pelvis angle subtracted from the maximum pelvis angle) during a drive averaged $10.9^o \pm 6.7^o$. The distribution of the pelvis angle changes is shown in Figure 22. Most of the angle changes were less than 4^o, however, 35 (27%) of the pelvis angle changes were larger than 6^o. The distribution of the maximum change in pelvic angle during the free drive is shown in Figure 23. Data on pelvic angle was available on 34 of the subjects, 12 had a change in pelvis angle greater than 10^o during the free drive.

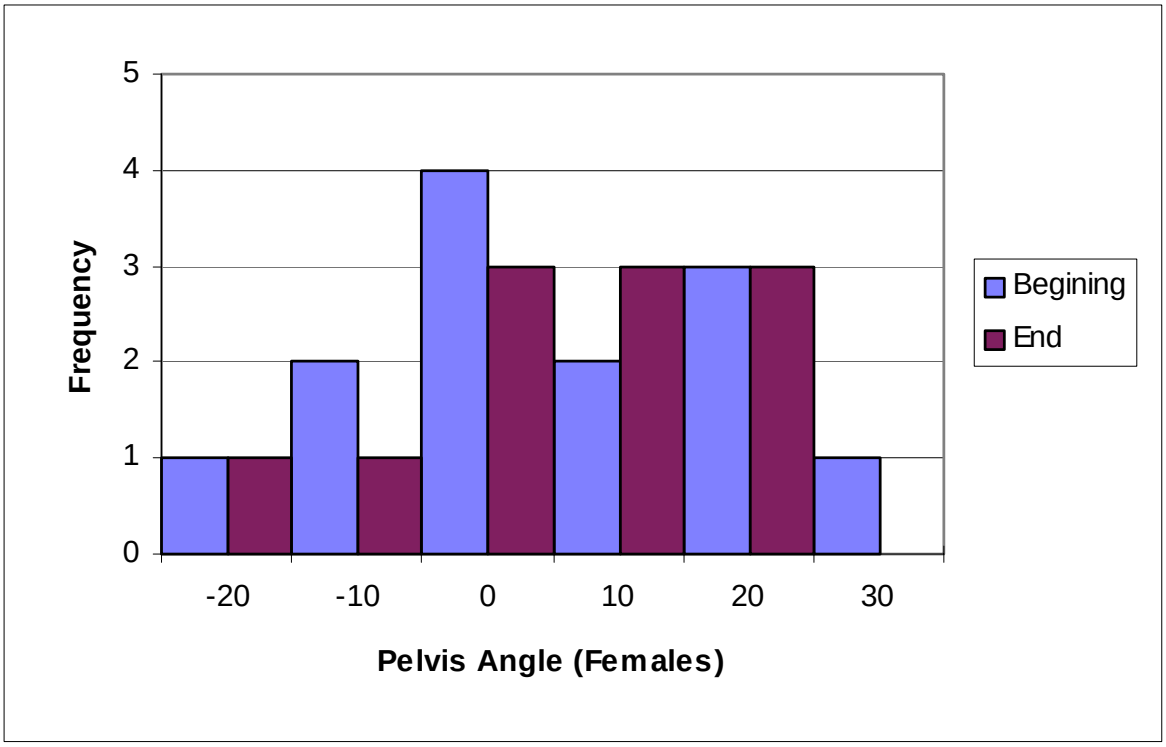

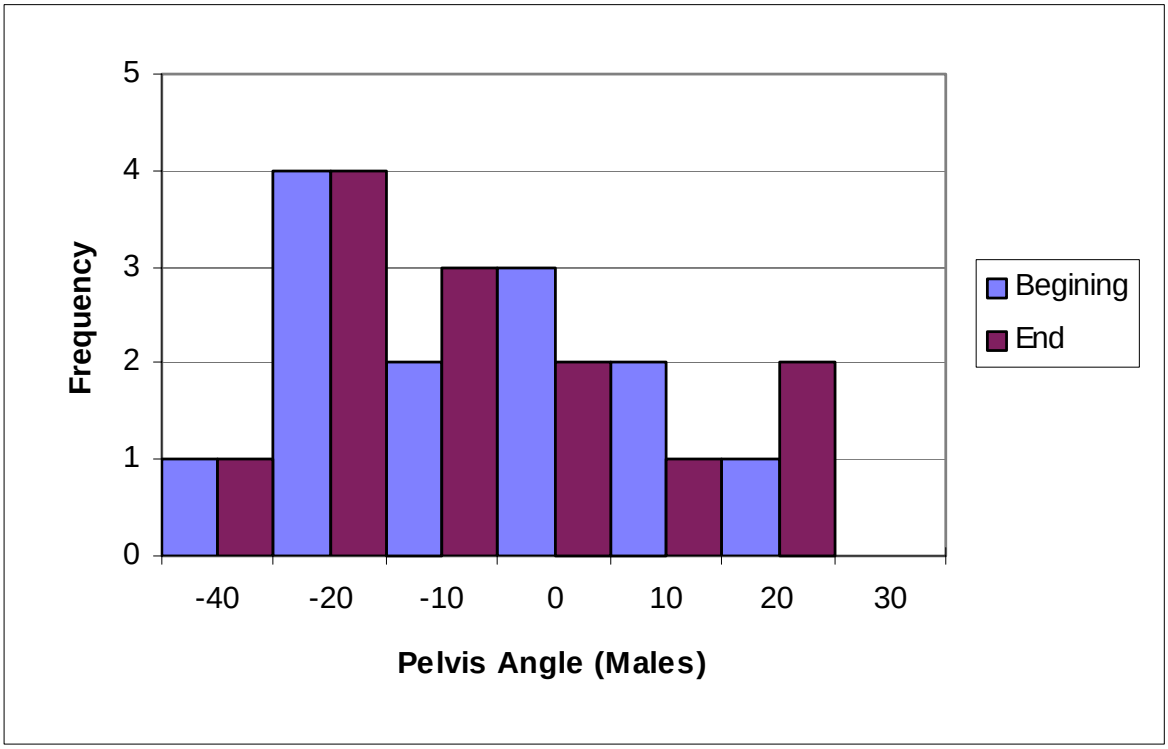

Figure 20 Distribution of pelvic angles for beginning and end of the modal position.

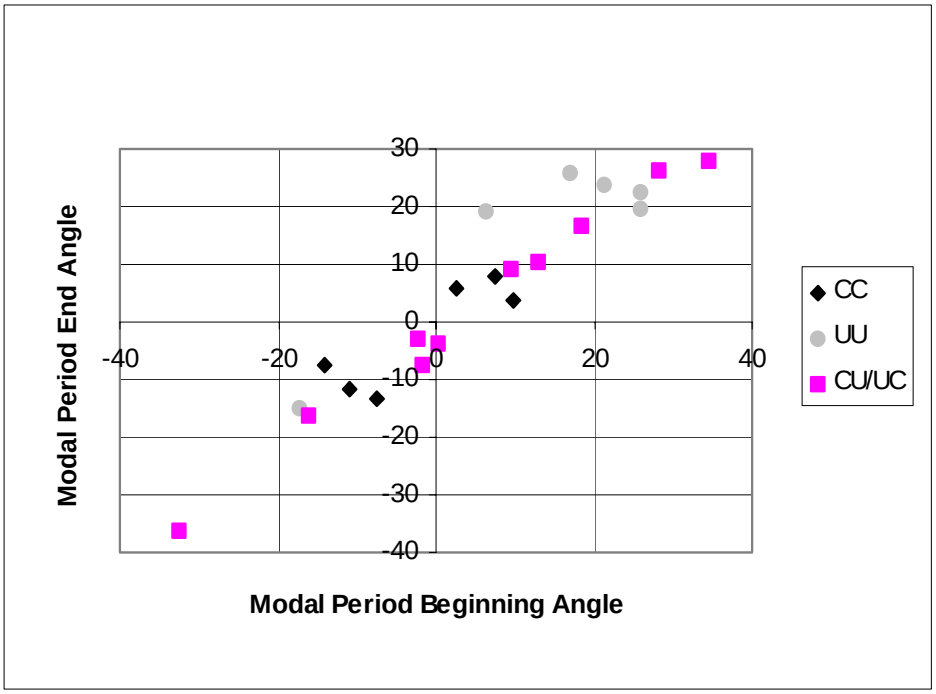

Figure 21 Pelvic angle at the beginning and end of the modal period of the free drive.

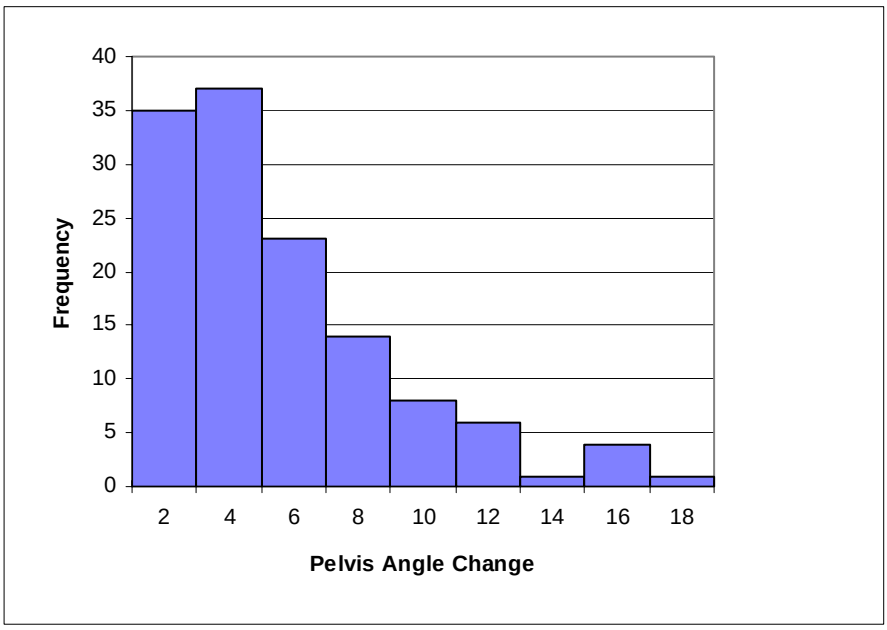

Figure 22 Frequency of changes in pelvic angle for the free drive.

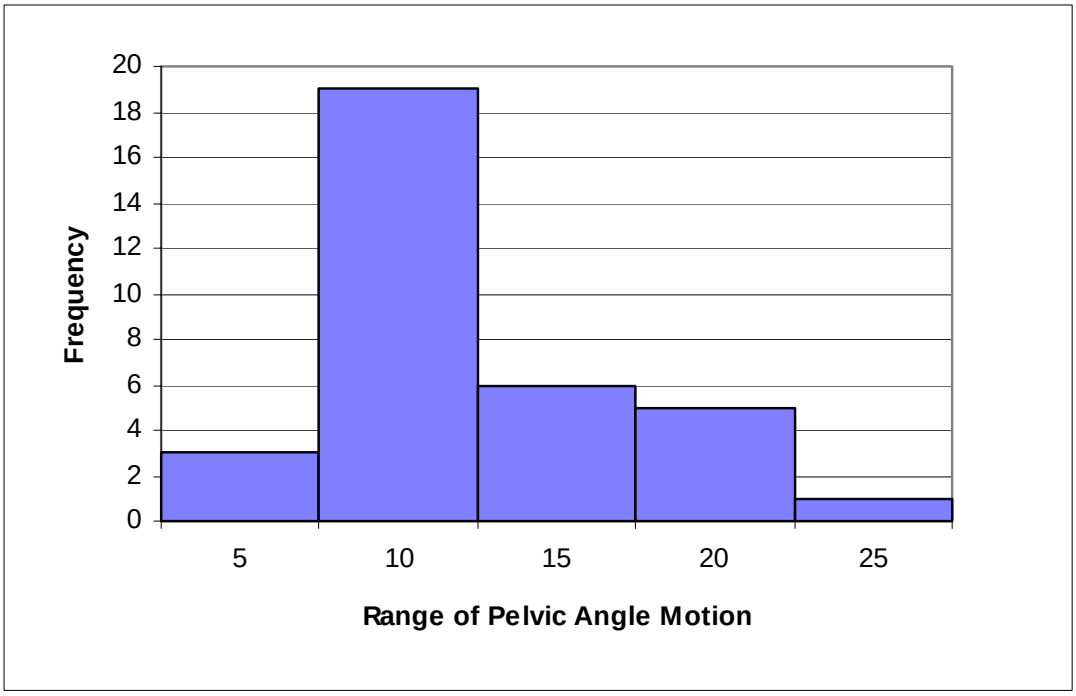

Figure 23 Distribution of the maximum pelvic angle change during the free drive.

Pelvis Angle During Fixed Seatback Drive

Pelvic angles for the fixed back drive are summarized in Table 11 and Figure 24. Males sat with their pelvis more reclined than females, but the differences were not statistically significant. In Figure 24, the distribution of pelvic angles is illustrated. More subjects had their pelves reclined while the seatback angle was smaller (more upright). This result was not expected and will be discussed in the next section.

	Pelvis Angle (Deg)	
	Ave	St Dev
Males Upright	-4.5	19.3
Females Upright	6.2	13.3
Males Reclined	-3.1	20.0
Females Reclined	5.5	14.5

Table 11 Pelvis angles for the upright and reclined seatback drives

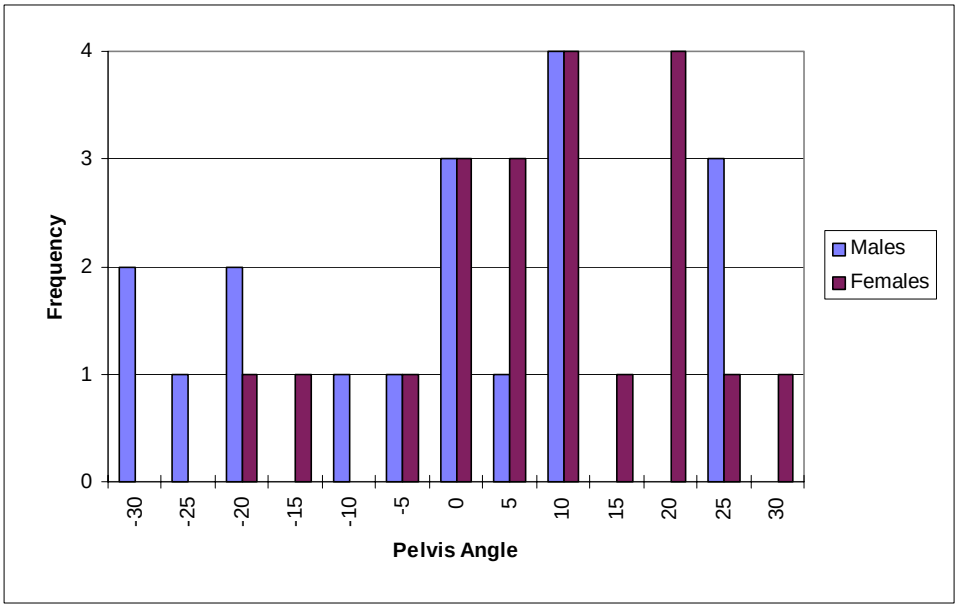

Upright Seatback Drive

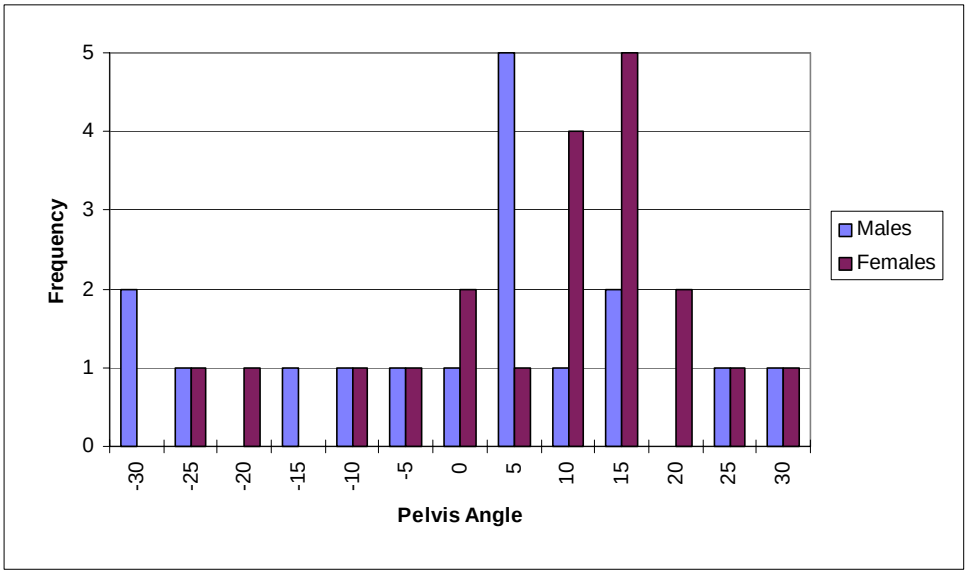

Reclined Seatback Drive

Figure 24 Distribution of pelvic angles during the fixed seatback drive.
(Top=Upright, Bottom=Reclined)

Lap Belt and the ASIS-AIIS Notch

Ideally the lap belt lies below the ASIS of the driver/occupant of any vehicle. If the person's posture is too slumped, then the chances for "submarining" (occupant sliding under the seat belt) increase in the event of an accident. There are two areas below the pelvis that can act like a "hook", holding the lap belt to the pelvis. The first is the ASIS-AIIS line, the second is the ASIS-Notch angle (see Figure 7). The orientation of these lap belt contact areas are given in Table 12. In general, the ASIS-AIIS line has a negative angle with

respect to the vertical (gravity) line. The more negative the angle, the greater the likelihood of submarining. The ASIS-notch angle is positive on average, indicating that the likelihood of submarining is smaller if the lap belt is securely beneath the ASIS-notch.

	Pelvis Angle ASIS-IT Line Relative to Gravity Line		**ASIS-AIIS Line Relative to Gravity Line**		**ASIS-Notch Angle Relative to Gravity Line**	
	Ave (deg)	**Std (deg)**	**Ave (deg)**	**Std (deg)**	**Ave (deg)**	**Std (deg)**
Beginning F	4.0	14.5	-9.5	14.5	16.2	14.5
Beginning M	-9.1	16.2	-22.4	16.2	3.1	16.2
End F	4.3	13.2	-9.0	13.2	16.5	13.2
End M	-10.2	17.9	-23.5	17.9	2.0	17.9

Table 12 Orientation of lap belt contact points during the beginning and end of the modal position.

C. Spine Posture

Estimating the spine posture of a subject requires that the sternum position be known relative to the pelvis. From Table 3 it can be seen that the sternum landmarks were often not visible by at least two cameras. The three-dimensional coordinates of the sternal2 landmark were not visible in 65% of the images and the Suprasternale was not visible in 39% of the images. As a result, the ability to estimate lumbar curvature was limited to those images that at least had the Suprasternale target visible. The number of lumbar curvature estimates for the modal position was reduced to nine complete sets of data.

The average lumbar curvature at the beginning of the modal period was -.29±.64 radians/spine height (SH) for females and 0.20±0.95 rad/SH for males. At the end of the modal period the lumbar curvatures became more lordotic (erect) with females having an average of -.43±.54 rad/SH and males an average of 0.08±.92 rad/SH. The differences between males and females were not statistically significant, but on average, females had slightly more lordotic lumbar spines for the free drive. The distribution of lumbar curvatures is shown in Figure 25 for the beginning and end of the modal period. The differences between the beginning and end of the modal period were small. The distribution of lumbar curvatures is shown for males and females in Figure 26 for the beginning of the modal period. The distribution of lumbar curvatures for the different comfort categories is shown in Figure 27. In all figures the units of lumbar curvature are rad/SH.

The change in lumbar curvatures between consecutive posture measurements is shown in Figure 28. The curvature changes are small between consecutive postures; however, if postural data was missing between two data collection periods, no change in lumbar curvature was calculated.

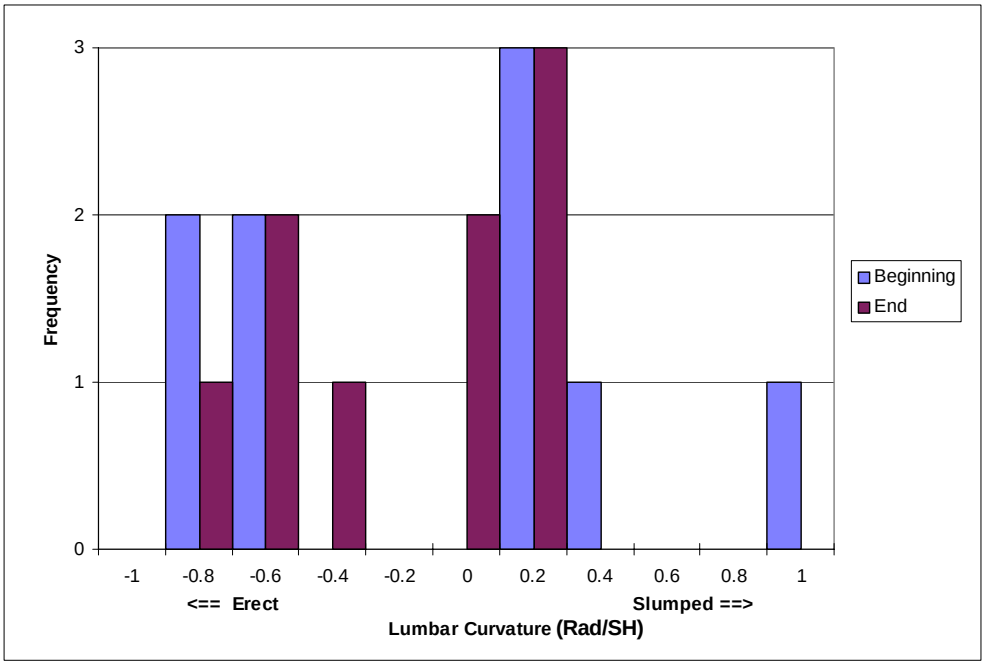

Figure 25 Lumbar curvature at the beginning and end of the modal period.

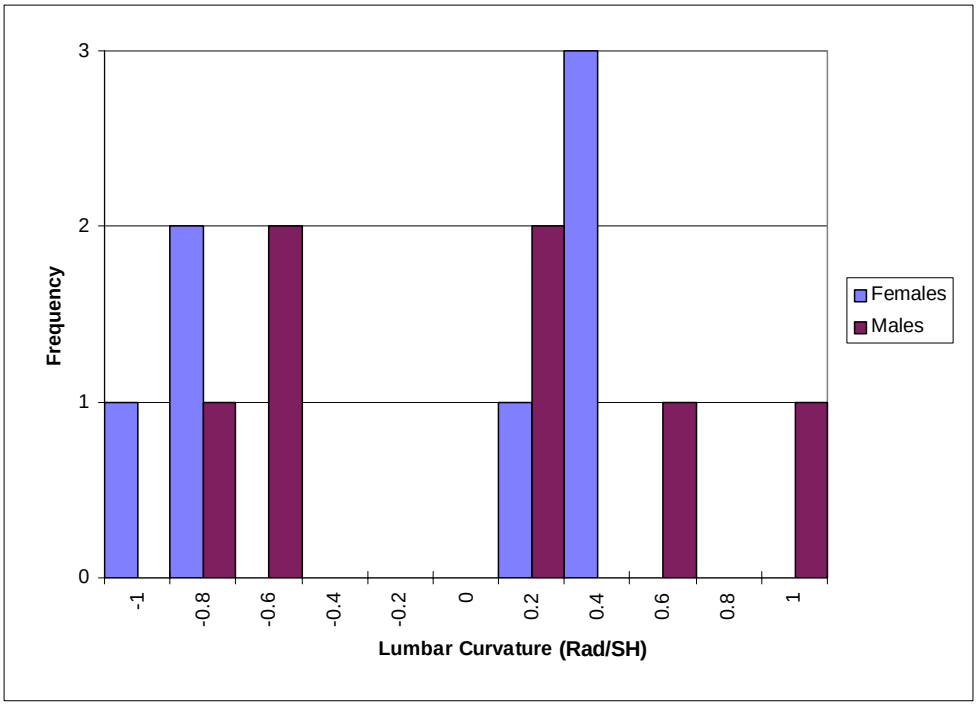

Figure 26 Lumbar curvatures of male and female subjects at the beginning of the modal period.

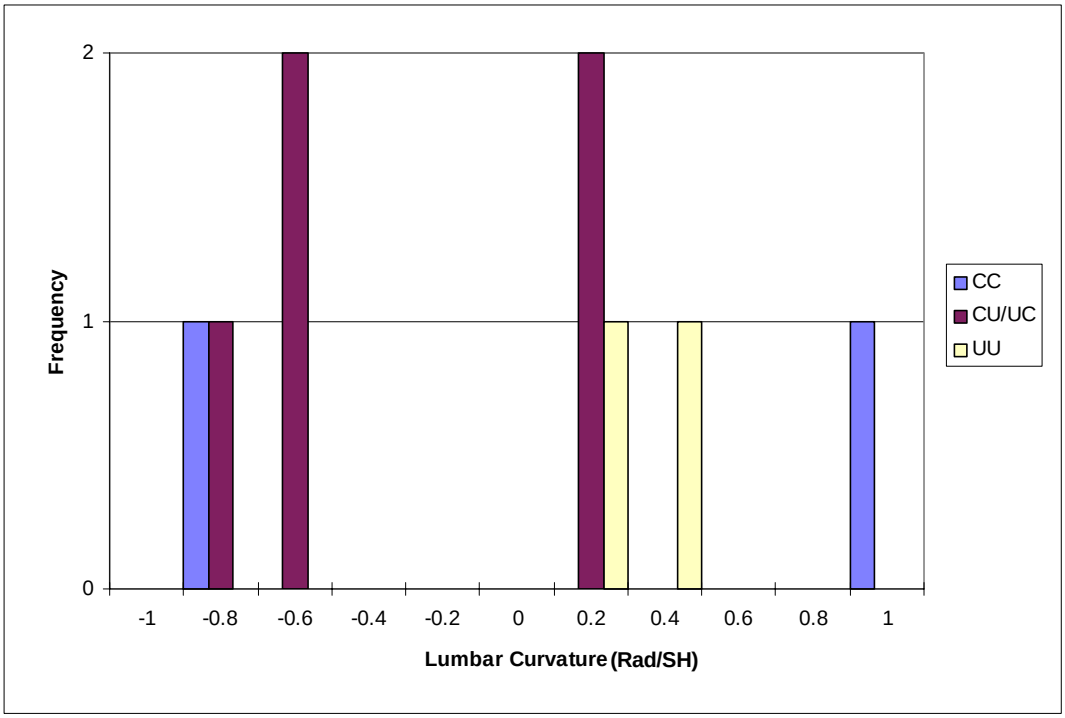

Figure 27 Lumbar curvature for each comfort group.

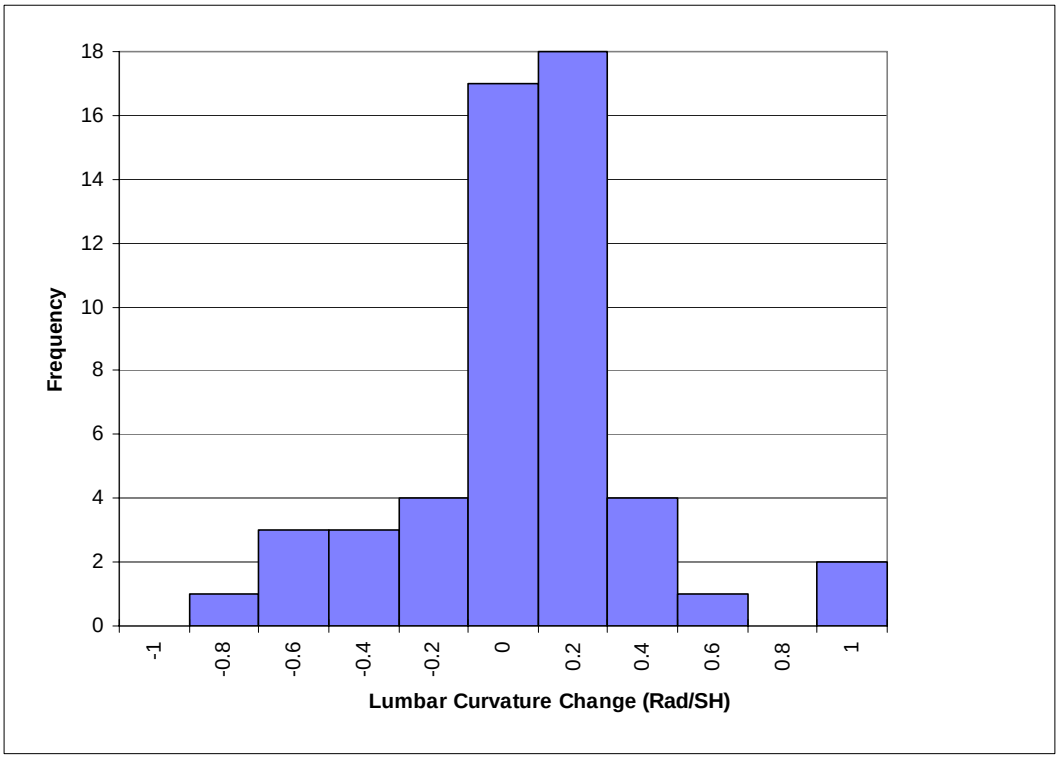

Figure 28 Changes in lumbar curvature during the free drive and the frequency with which they occur.

The data for the upright and reclined drives are summarized in Table 13. The average lumbar curvature was more lordotic for the reclined drive than for the upright drive (p=0.047). Males had greater lordotic curvatures than females although the differences were not statistically significant. Both sexes had greater lumbar extension with the seat back reclined. These results were the reverse of what was expected. We suspect that the reclined seat back position was too reclined, requiring the subjects to modify their posture in order to see through the windshield. These results will be discussed in more detail in the discussion section of this report.

The distribution of lumbar curvatures is given for the upright and reclined drives in Figure 29. The reclined drive had a bimodal distribution, with one peak near zero and the other near -2 rad/SH. The upright drive is closer to a normal distribution, with most of the postures near zero rad/SH.

The female and male results are illustrated for the upright drive in Figure 30 and for the reclined drive in Figure 31. For the upright drive, the male distribution is bimodal with a large cluster near zero and a second peak at about -2.5 rad/SH, while the female distribution is closer to a normal distribution. In addition, the male distribution is skewed toward the extended posture. For the reclined drive, both sexes have their distribution skewed toward the extended posture

	Total	Total	F	F	M	M
	Average	St Dev	Average	St Dev	Average	St Dev
Upright	-0.10	1.45	0.17	1.55	-0.46	1.26
Reclined	-0.64	1.01	-0.51	0.87	-0.81	1.17

Table 13 Average curvatures for upright and reclined drives. Units are rad/SH.

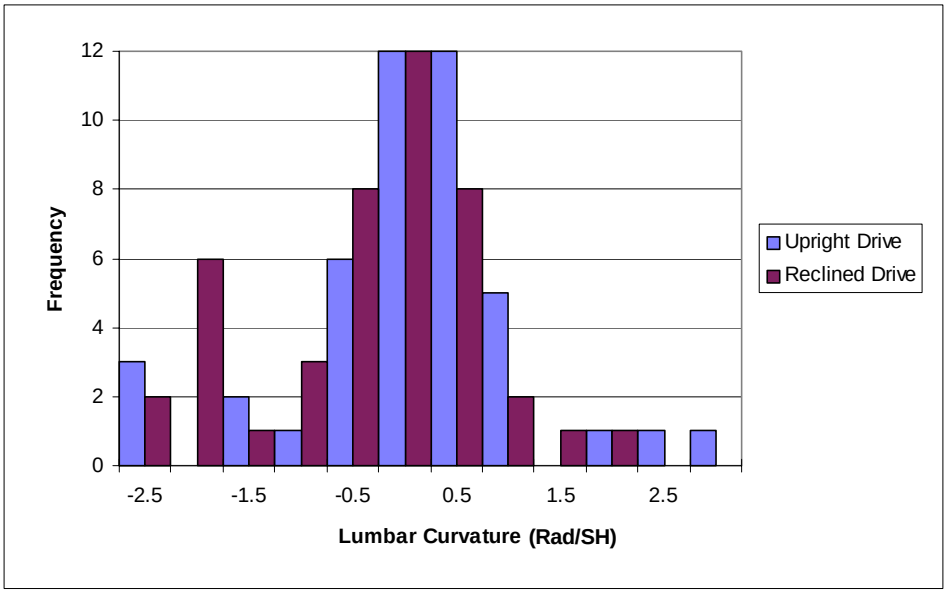

Figure 29 Lumbar curvature distribution for the upright and reclined drives. Units are Rad/SH.

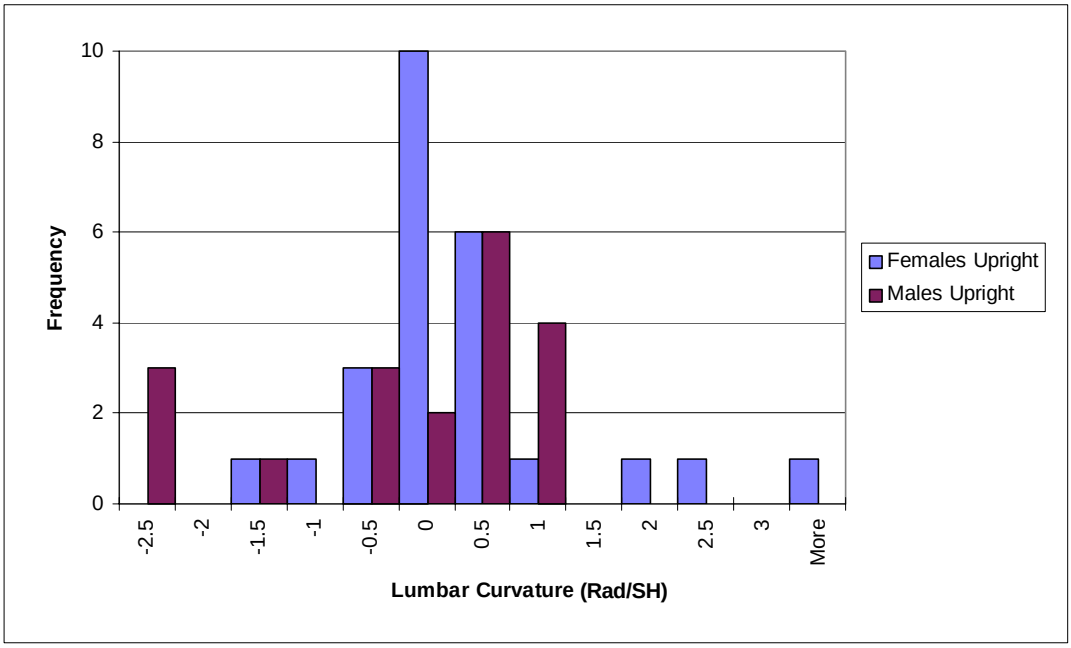

Figure 30 Lumbar curvatures for males and females during the upright drive.

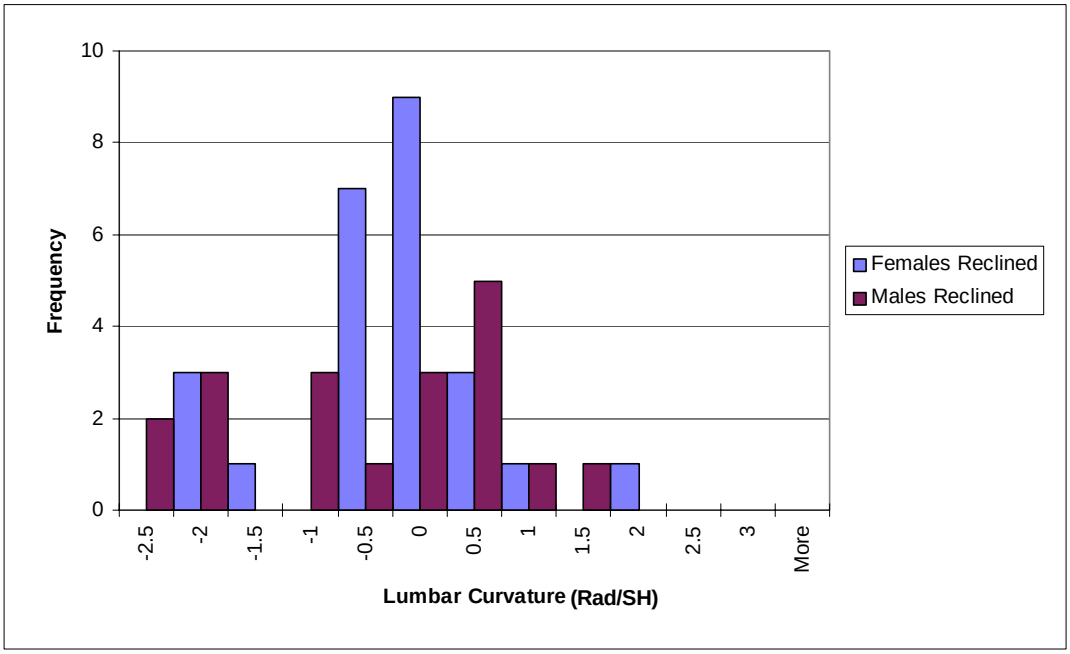

Figure 31 Lumbar curvatures for males and females during the reclined drive.

D. Body Linkage Angles and Joint Angles

Joint angles and the angles formed by body linkages were defined in Section II of this report (Figure 8 - Figure 11). The results are summarized in Table 14 for the beginning and end of the modal period.

	Beginning	Beginning	End	End	Beginning	Beginning	End	End	Beginning	Beginning	End	End
	Total Ave	Total Std	Total Ave	Total Std	F Ave	F Std	F Ave	F Std	M Ave	M Std	M Ave	M Std
Eye-neck-hip-2d	119.3	7.4	119.0	8.3	120.7	8.3	120.6	8.6	117.9	6.3	117.2	8.2
Eye-acromion-hip-2d	142.5	11.1	142.5	8.7	144.9	13.1	143.2	9.8	139.9	8.2	141.6	7.5
neck-hip-zx	14.3	5.7	14.3	5.8	13.7	6.3	14.0	6.1	15.0	5.2	14.5	5.7
acromion-hip-zx	12.5	5.9	12.6	6.3	11.2	6.6	11.9	7.0	14.1	4.8	13.2	5.7
acromion-neck-yz	29.6	20.7	34.4	30.1	33.2	27.9	34.8	30.8	25.5	5.3	34.0	30.7
acromion-neck-yx	16.6	23.6	21.5	33.9	20.9	31.6	21.3	34.6	11.7	5.9	21.7	34.5
acromion-elbow-zx	140.2	18.0	141.1	17.2	142.3	18.6	147.3	18.4	138.0	17.7	134.4	13.3
acromion-elbow-wrist-2d	105.8	19.3	107.2	20.4	100.2	19.1	101.5	22.8	111.4	18.3	112.9	16.4
acromion-elbow-wrist-3d	103.7	18.4	104.9	18.7	98.5	18.4	98.8	20.3	108.9	17.4	111.0	15.2
neck-hip-knee-2d	98.6	7.0	97.9	7.4	97.7	6.6	97.2	6.9	99.5	7.4	98.5	8.0
acromion-hip-knee-2d	96.7	7.3	96.4	7.5	95.0	7.2	95.3	7.5	98.7	7.1	97.6	7.7
acromion-hip-knee-3d	92.4	6.2	91.9	6.5	92.3	6.7	92.9	7.3	92.6	5.9	90.8	5.6
hip-knee-ankle-2d	121.2	6.9	119.4	8.3	123.3	6.4	121.9	8.3	117.1	6.5	115.2	7.3
hip-knee-ankle-3d	119.6	7.9	118.4	8.6	122.6	7.1	121.4	8.0	113.6	5.9	113.2	7.8
hip-knee-xz	5.8	3.8	6.5	4.1	5.7	3.4	6.6	4.1	5.9	4.2	6.4	4.3
elbow-acromion-hip-3d	36.5	12.5	36.6	12.5	35.4	13.9	33.9	14.6	37.6	11.3	39.3	9.8
Thigh Splay (hip-kneeyz)	15.6	7.4	15.9	8.8	10.6	4.7	8.5	4.1	20.0	6.5	21.5	7.1
knee-ankle xz (calf angle)	52.2	4.8	52.2	5.1	51.7	5.5	51.7	5.8	53.2	3.4	53.1	3.8
knee-ankle xy (calf splay)	0.0	13.6	-3.2	12.0	-5.5	12.8	-6.5	10.7	10.3	8.2	3.4	12.8

Table 14 Joint angles and linkage angles for the beginning and end of the modal period.

E. Eye Point During Modal Period

The average eye point location for the modal period of the free drive is summarized in Table 15. As would be expected, males had a higher eye point than females, and for both sexes the eye point height decreased by the end of the modal period. The average eye point positions were compared to the location of the X-Z datum line intersection of the eyellipse taken from the vehicle drawing. The average eye locations are illustrated in Figure 19 along with the location of H-point, D-point and the un-deformed seat contour.

	Eye Pt Beginning		Eye Pt End	
	X	Z	X	Z
F Ave	78.05683	828.7137	100.3093	825.5131
F St Dev	86.93282	30.31727	93.03285	30.8831
M Ave	65.13142	868.6585	78.30721	858.7801
M St Dev	67.04373	27.99903	83.07889	25.52055
	Eyellipse XZ Datum Lines Intersection Point			
	X		Z	
	59.6		843.4	

Table 15 Eye point location during modal period

IV Discussion

Target Visibility

In order to determine the three-dimensional position of a target, it must be visible from at least two cameras. There were a total of 448 image sets examined for all subjects for the fixed and free back drives. Of these image sets (4 video pictures per image set) the second sternum landmark was not visible on any camera 293 times. The ankle was not visible on 237 image sets and Suprasternale was not visible on 176 image sets. The shoulder strap often covered the Suprasternale and the second sternum target. During the drive, the ride techs were instructed to view each image set to insure that all targets were visible in at least two cameras, before saving the image files to disk. However, the monitors were LCD monitors, selected for low power usage and for safety reasons. These monitors could not show the detail required identifying each target and, as a result, the ride techs only inspected images for exposure quality. Losing the chest targets severely limited our ability to determine chest orientation, resulting in a loss of our ability to estimate spinal posture for several subjects. In future studies, the chest landmarks will be modified so that the shoulder strap does not interfere with target visibility. In addition, we need to investigate methods for improving the video images so that the ride techs can monitor target visibility.

The ankle target was not visible for many subjects due to the extreme rotation of the shank and foot. Several subjects externally rotated their shank and supinated their foot to such a degree that their lateral malleolus (landmark for the ankle target) lay at or near the floorboard of the car, or too close to the centerline tunnel. As a result, the ankle target was not visible on more than one camera and many times not visible on any camera. Due to the poor image quality when viewed on the LCD monitors, the loss of this target was not noted until the pictures were viewed later. We assume that these subjects prefer to sit in this manner and that asking subjects to modify their foot orientation would interfere in our efforts to monitor their posture. In future studies we will investigate methods for overcoming this problem; possibly by placing the ankle target at a different location, so that large external rotations do not hide it.

Error Analysis

The accuracy of the 3DAQ system has been shown to be on the order of 0.05mm-5.5mm (Figure 13). However, the system accuracy is also dependent on the subjective decision of each user as to the exact point used to define a target. Although the 3DAQ system has an automated routine for locating the center of an ellipse, the actual shape of the targets is rarely elliptical, and thus this routine is of limited value. The subjective decisions of each user, then becomes an issue of some importance.

The results of three trained users measuring landmarks on one subject are listed in Table 5. The standard deviation of the link lengths between two targets provides an estimate of the error. The landmarks having the highest degree of reproducibility were the Suprasternale and the second sternum targets (SD less than 2mm). The ASIS and the ankle targets had the highest degree of variability, with link length involving these two targets having SD ranging from 5 to 16mm.

Another means of estimating error is to average link lengths for multiple image sets of each subject, using the average link length as the best estimate of the mean and

examining the absolute error between the mean and all other measurements. The results of this analysis are illustrated in Table 6, Table 7 and Figure 14. The vast majority of our error estimates are below 5mm (82.8%), with 98.7% being below 10mm. The link length having the largest overall degree of variability was the ASIS-knee link (average absolute error = 6.7±5.7mm). It must be pointed out that this link is not rigid, since when the thigh moves it rotates about the hip joint. The ASIS-knee link is only an estimate of a rigid body and we do not know how much error is due to the non-rigid nature of the link. The next sternum landmarks had the greatest consistency, with an average absolute error estimated at 1.5±1.3mm. All other links had average absolute errors below 3mm, indicating that the 3DAQ system is very reliable.

Pressure Map Quality

The quality of the pressure mat images is definitely affected by sex. Males tend to have more discernible pressure peaks on their pressure mappings than females ($p=0.005$). This finding leads us to speculate that pressure map quality is a function of hip-breadth. However, a regression of pressure map quality against hip breadth has an $r^2 = 0.12$, indicating no correlation between the two variables. We suspect that it is not the hip breadth that causes such a marked difference in pressure map quality so much as it is the amount and type of tissue between the ischial tuberosity and the seat surface. Women have more adipose tissue in the buttock region and this could affect the pressure map quality, reducing the slope of the pressure gradient and making it more difficult to determine the ischial tuberosity location.

Locating the Pelvis in the Free Drive

For the free drive, we report on the pelvis position using the modal period of each subject. The modal period is defined based on the time a given subject sat in a seat position longest [25]. We report on the position of the pelvis for the beginning and end of the modal period.

The location of the hip joints for our subjects was compared to the location of the H-point window in Figure 15. Moving the H-point from the seat in the design position to the extremes of all possible seat travel positions generated an H-point window. The resulting path is the H-point window. All subjects had their hip joints well forward of the design location for H-point, and many subjects had their hip joints well above the H-point window maximum height. It must be noted that this data reports the position of the subjects' hip joints without adjusting for seat position. Since the H-point window defines the perimeter of all possible H-point locations for the seat travel, the subjects' hip joints should lie within the H-point window. For this seat, the subjects' hip joints do, for the most part, lie within the H-point window, but a number of them lie considerably above it.

We defined a similar window for D-point and compared that to the location of our subjects' ischial tuberosities (Figure 16). The D-point window for this seat is low and posterior compared to the ischial tuberosity locations for our subjects. Most subjects were not even in the boundaries of the D-point window.

In order to understand the pelvic data in terms of the seat design template Oscar, we calculated the hip joint and ischial tuberosity locations relative to the seat design position. All results are given with respect to the seat coordinate system, and the measured position

of H-point as measured by the H-point machine. The results for our subjects hip joint and ischial tuberosity locations are summarized in Table 9.

The location of H-point and D-point compared to the subjects' hip joints and ischial tuberosities are illustrated in Figure 17 and Figure 18. All subjects sat well forward of the design position of both H-point and D-point and most subjects sat well above the D-point. The average hip joint and ischial tuberosity locations are more than 50mm further forward than the design positions for H and D points (Figure 19).

The Oscar template assumes continuous contact with the seatback and seat cushion and, as a result, the placement of the H-point machine (3D Oscar) requires not only continuous contact with the seat surface but also considerable compression of the foam. Thus, the design H-point and the corresponding measurements from the H-point machine are unrealistic representations of seated posture.

The differences in D-point location not only represent translation differences between our subjects and Oscar, but are also due to fundamental anatomical errors in Oscar. The Oscar template has D-point coupled to the thigh instead of attached to the pelvis. Subjects were measured in their preferred posture, which ranged from slumped to erect, while Oscar represents a neutral posture. Thus, we expect a degree of scatter to the ischial tuberosity location, but if the Oscar estimate for D-point is reasonable, then that scatter should center at or near D-point. The fact that the D-point location for this seat is too far posterior indicates that there is a real need to re-evaluate the Oscar design template. Given the structure of the seat, it is very difficult for a living person to actually place their ischial tuberosities near the design D-point.

For this seat, subjects sat with their ischial tuberosities almost directly beneath their hip joints (Figure 19), with males slightly reclined and females sitting more upright (Table 10). The distribution of pelvic angles is shown in Figure 20 and shows that more males sat with their pelvises leaning further back while more females sat with their pelvises upright. These facts help explain why the average female ischial tuberosity location is deeper in the seat than the males. When seated more upright, more weight passes through the ischial tuberosities, whereas when seated in a reclined position, more of the body weight is carried by the seatback and some of the weight is distributed through the sacrum, reducing the depth of penetration.

The same pattern of pelvis angle orientation held true for the fixed back drive as well. Males tended to sit in a more reclined posture than females with an average difference ranging between 8^o and 10^o (Table 11). An interesting aspect of the fixed drive is that there was a non-significant difference in the pelvic angle between the upright and reclined drives. We expected to find that subjects had their pelvis more reclined during the reclined seatback drive. However, the opposite was true. Both males and females sat slightly more upright during the reclined seatback drive. During this drive, the seatback angle was held fixed with an angle of 30^o from the vertical. We suggest that this was too reclined and that subjects overcame the backrest angle by using muscle contraction to sit more upright.

Lap Belt and the ASIS-AIIS Notch

During a front-end collision it is not uncommon for a person to "submarine" below the seatbelt, nullifying any restraining forces the seatbelt could have applied to prevent

injury. One key aspect to preventing submarining is the relationship between the seatbelt ant the ASIS of the pelvis. If the ASIS is below the seatbelt, the notch below the ASIS can act like a hook, reducing the chances of the torso slipping beneath the seatbelt. However, if a person is greatly slouched, then the ability of the ASIS to slide beneath the seatbelt increases, and so do the chances of submarining. The more vertical the ASIS-AIIS region of the pelvis, the less chance there is of a person submarining.

The biomechanics of submarining are very complex; depending on the direction of impact, the posture, body proportions and pelvic shape of the victim. One aspect of the pelvic area that is directly affected by excess weight is the ASIS-AIIS region. The ability of the notch beneath the ASIS to hook a seatbelt is reduced with extra tissue or clothing in the area. In our study, the angle of the ASIS notch is steeper than the ASIS-AIIS region (see Figure 7), leaning further forward by an average of about 16^o for females and 3^o for males (Table 12). Thus, even in the more reclined posture of the males, the ASIS notch is more likely to hook the seatbelt. However, excess tissue and clothing over this area are likely to reduce the effectiveness of this notch so that submarining is then more dependent on the angle of the ASIS-AIIS region.

In this study we estimated the angle of the ASIS-AIIS region and found that for males, this region averages more than twice the inclination of females (averaging approximately -22^o for females compared to -9^o for males). This indicates that it would be easier for submarining to occur for males (Table 12). This difference is primarily due to the fact that men sat with their pelvis in a more reclined posture.

Spine Posture

We have developed a method for estimating the spine posture based on the position of the sternum relative to the pelvis [43]. This model requires that the angle of the pelvis be known as well as the position of at least one point on the sternum. Due to data collection problems the sternum targets were not visible in about one third of the image sets collected. This greatly reduced our ability to predict lumbar posture for several subjects. However, the results for the lumbar spine curvature estimates support the findings of the pelvis posture: males sat with a more slouched posture while females sat with a slightly lordotic lumbar spine (Table 10, Figure 25 and Figure 26). In addition, by the end of the modal period both males and females had become slightly more erect than they were at the beginning of the modal period.

For the fixed seatback drive, subjects sat more erect when they were in the reclined seatback position (Table 13 and Figure 29). Males sat more erect for both the upright and reclined seatback positions, than their posture was during the modal period of the free comfort drive. The differences were not statistically significant and the numbers involved were small, so we cannot rule out measurement and sampling errors. The pelvic angles (Table 11) reported for the fixed back drive indicate the opposite trend: both males and females had more reclined pelvises in the fixed back drives than in the free drive. However, there were fewer subjects available for estimating the lumbar curvature, thus the sample available may have biased the spine curvature results.

Joint Angles and Body Linkage Positions

All angles listed in Table 14 are with respect to the seat coordinate system. Thus to obtain the angle relative to the car coordinate system the 7.5^o rotation of the seat has to be

accounted for. This 7.5^o correction is only relevant for angles of body linkages such as the torso angle (angle of the shoulder-hip line) or the thigh angle (angle of the hip-knee line).

The current SAE template, Oscar, uses the hip and shoulder joints to define the torso angle. However, the shoulder joint does not have a fixed center of rotation, but is a complex mechanism with the point defined by Dempster [11] moving significantly relative to the torso. We used the point defined by Dempster as the center of the shoulder joint and compared the angle of the shoulder-hip line to the angle of the neck-hip line. The neck point was defined as the junction between the shoulder and neck. Both of these lines gave similar angles for torso inclination and both had similar standard deviations (Table 14), indicating that using the shoulder-hip joint provides the same torso inclination as using the neck-hip joint line. The fact that the standard deviations were similar indicates that although shoulder motion has the potential to be large, subjects sat with their shoulder joints in similar positions. Males sat slightly (1^o - 3^o) more reclined than females, but the difference was not significant. This more reclined posture is in agreement with our pelvic findings.

The head posture was defined using the eye-neck-hip points as well as the eye-shoulder-hip. Both measurements had similar results, although the measurement using the shoulder joint had more variability due to the fact that the angle of the eye-shoulder line to be sensitive to small changes in shoulder position. Males sat with their heads about 3^o closer to their torsos than females. The fact that they were slightly more reclined required them to tilt their head more in order to keep their eyes level with the horizon.

Males sat with about 10^o more elbow extension than females. That is, females sat with their shoulders closer to the steering wheel and with their elbows closer to being at right angles. Again, this is an indication that the females were sitting more upright than the males.

The torso-thigh angle was measured using the neck-hip-knee as well as the shoulder-hip-knee points. Both give similar results, with the males having between 1^o-3^o more of an inclination than females. In addition, both males and females are within a few degrees of the design position of Oscar (99^o). The thigh inclination (hip-knee angle) was the same for both males and females, at about 6^o, indicating that both sexes preferred this as their thigh angle.

Design posture for the knee angle was 128^o, which is significantly larger than the angle preferred by our subjects. Males sat with a knee angle of about 115^o while females sat at about 122^o. This may be due to the fact that most males could not move the seat far enough back and thus had to sit with a smaller knee angle, while females could adjust the seat to achieve a larger knee angle.

We also investigated the thigh splay and calf splay. Males sat with their thighs splayed at about 20^o while females were at about 10^o. The calf splay for women was about negative 5^o while for men it was a positive 10^o. Since men sat with their thighs relatively splayed apart, they had to orient their lower leg so that their calf splay was sufficient to orient the foot over the gas pedal. Due to etiquette, women sit with their thighs closer together and have to splay their lower legs in the opposite direction in order to orient the foot over the gas pedal.

Eye Point

We compared the eye point to the X-Z datum line intersection point on the eyellipse (Table 15 and Figure 19). Both men and women were close to this point, with men being slightly higher and women being slightly lower, as would be expected.

References

[1] Andersson, Gunnar B. J. Loads on the Spine during Sitting. Chapter 27. In: Nigel Corlett, John Wilson, & Ilija Manenica (eds) The Ergonomics of Working Postures. Models, Methods and Cases. Philadephia, Taylor & Francis, 1986, pp.309-318.

[2] Adams MA and Hutton WC "The effect of posture on the lumbar spine." J Bone & Jt Surg. 67-B(4):625-629.

[3] Hall MAW "Back pain and car-seat comfort." Appl Ergo. 3:82-91, 1972.

[4] Heliövaara, M "Occupation and risk of herniated lumbar intervertebral disc or sciatica leading to hospitalization." J Chron Dis 40(3):259-264, 1987.

[5] Kelsey JL, Githens PB, O'Conner T, Weil U, Calogero JA, Holford TR, White III AA, Walter SD, Ostfeld AM, and Southwick WO "Acute prolapsed lumbar intervertebral disc. An epidemiologica study with special reference to driving automobiles and cigarette smoking." Spine 9(6):608-613, 1984.

[6] Troup JDG "Driver's back pain and its prevention. A review of the postural, vibratory and muscular factors, together with the problem of transmitted road-shock." Applied Ergonomics 9(4):207-214, 1978.

[7] Andersson BJG, Örtengren R, Nachemson A, and Elfström G "Lumbar disc pressure and myoelectric back muscle activity during sitting. IV. Studies on a car driver's seat." Scand J Rehab Med 6:128-133, 1974.

[8] Hosea TM, Simon SR, Delatizky J, Wong MA, Hsieh C-C "Myoelectric analysis of the paraspinal musculature in relation to automobile driving." Spine 11(9):928-936, 1986.

[9] Reed MP, Schneider LW, and Ricci LL Survey of auto seat design recommendations for improved comfort. Technical Report, UMTRI-94-6, The University of Michigan Transportation Research Institute, Ann Arbor, MI, 1994.

[10] Geoffrey SP "A 2-D Mannikin -- The inside story. X-rays used to determine a new standard for a basic design tool." SAE #267A, SAE International Congress, Detroit, 1961.

[11] Dempster WT Space Requirement of the Seated Operator: Geometrical, kinematic, and mechanical aspects of the body with special reference to the limbs. WADC Technical Report 55-159, Wright Air Development Center, Ohio, 1955.

[12] Stoudt HW, Damon A, McFarland R, and Roberts J "Weight, height, and selected body dimensions of adults." National Center for Health Statistics, Series 11, Number 8, U.S.Department of Health, Education, and Welfare, 1965

[13] Andersson GBJ, Murphy RW, Örtengren R, and Nachemson AL "The influence of backrest inclination and lumbar support on lumbar lordosis." Spine 4(1):52-58, 1979.

[14] Beneck GJ Influence of motot vehicle seat geometry on pelvic inclination. Master's Thesis, Michigan State University, 1990.

[15] Keegan J 1953 "Alterations of the lumbar curve related to posture and seating." J Bone & Joint Surgery 35-A:589-603.

[16] Bendix T "Sitting postures -- a review of biomechanic and ergonomic aspects." Manual Medicine 2:77-81, 1986.

[17] Reynolds HM Erect, Neutral and Slump Sitting Postures: A study of the torso linkage system from shoulder to hip joint. Final Report, AL/CF-TR-1994-0151. Air Force Materiel Command, Wright-Patterson Air Force Base, Ohio, 1994.

[18] Nachemson A "The possible importance of the psoas muscle for stsabilization of the lumbar spine." Acta Orthop Scand 39;47-57, 1968.

[19] Roe, RW "Occupant packaging," pp 11-42. Chapter 2 in: B Peacock and W Karwowski (eds) Automotive Ergonomics. Taylor & Francis, Washington, D.C., 1993.

[20] SAE Handbook, Volume 4, On-Highway Vehicles and Off-Highway Machinery. SAE, Inc., 400 Commonwealth Drive, Warrendale, PA 15096, 1984.

[21] Rebiffé R ["The driving seat. Its adaptation to functional and anthropometric requirements."] "Son adaptation aux exigences fonctionnelles et anthropometriques," pp 132-147. In E Grandjean (ed) Proceedings of the Symposium on Sitting Posture. London, Taylor & Francis, Ltd., 1969.

[22] Babbs FW "A design layout method for relating seating to the occupant and vehicle." Ergonomics 22(2):227-234, 1979.

[23] Thornton W "Chapter I. Anthropometric changes in weightlessness." In: Staff of Anthropology Research Project (eds.) Anthropometric Source Book. Volume 1: Anthropometry for Designers. NASA Reference Publication 1024, NASA, Scientific and Technical Information Office, 1978.

[24] Diebschlag W, Heidinger F, Kurz B, Heiberger R "Recommendation for ergonomic and climatic physiological vehicle seat design." SAE #880055. Paper presented at SAE International Congress and Exposition, Detroit, Michigan, 1988.

[25] Reynolds HM, Neal D, Kerr R "The Initial position and postural attitudes of driver occupants, Seat Position." Technical Report ERL-TR-95-006. Ergonomics Research Laboratory, Michigan State University, 1996.

[26] Eppler M, Reynolds HM, Zhang L "The initial position and postural attitudes of driver occupants, comfort." Technical Report ERL-TR-95-008. Ergonomics Research Laboratory, Michigan State University, 1995.

[27] Brodeur R, Cui Y, Reynolds HM "The initial position and postural attitudes of driver occupants, H-point and D-point in the pelvis." Technical Report ERL-TR-95-003. Ergonomics Research Laboratory, Michigan State University, 1995.

[28] Eppler MM The development of a method to encode body movement of automotive vehicle operators. Master of Arts Thesis, Department of Human Environment and Design, Michigan State University, 1995.

[29] Reynolds HM, Brodeur R, Eppler M, Neal D, Rayes K, Kerr R, Stockman G "The Initial Position and Postural Attitudes of Driver Occupants. Experimental Protocol. ERL-TR-95-001rev. Technical Report, Ergonomics Research Laboratory, Michigan State University, East Lansing, MI. 1995.

[30] Stockman G, Chen J-L, Cui Y and Reynolds H "Measuring body points on automobile drivers using multiple cameras. Accepted for publication, Image and Vision Computing. 1996.

[31] Cappozzo A "Gait analysis methodology." Human Movement Science, 3: 27-50, 1984.

[32] Cui Y, Weng J and Reynolds H, "Estimation of ellipse parameters using optimal minimum variance estimator." Pattern Recognition Letters. 17:309-316, 1996.
[33] Brodeur RR, Cui Y and Reynolds HM, The initial position and postural attitudes of driver occupants, H-point and D-point in the pelvis, ERL-TR-95-003, Ergonomics Research Laboratory, 1995.
[34] Anderson BD and Moore JB Optimal Filtering. Englewood Cliffs, NJ: Prentice-Hall, 1979.
[35] Broida TJ and Chellappa R "Estimation of object motion parameters from noisy images." IEEE Trans. PAMI, 8(1):90-99, 1986.
[36] Ellis T, Abbood A and Brillault B "Ellipse detection and matching with uncertainty." Image Vision Comput. 10(5):271-276, 1992.
[37] Gutman P and Velger M "Tracking targets using adaptive Kalman filtering." IEEE Tran. on Aerospace and Electronic Systems, 26:691-698, 1991.
[38] Zhang Z and Faugeras O, "Three-dimensional motion computation and object segmentation in a long sequence of stereo frames." International Journal of Computer Vision, 7:211-241, 1992.
[39] Luenberger DG Optimization by Vector Space Methods. Wiley, New York, 1969.
[40] Blostein SD and Huang TS "Algorithms for motion estimation based on 3-D correspondences." In W. Martin and J. K. Aggrawal (eds) Motion Understanding,. Norewell, MA: Kluwer, 1988.
[41] Elbert TF Estimation and Control of Systems. New York, Van Nostrand Reinhold, 1984.
[42] Reynolds HM, Snow CC, Young JW. "Spatial geometry of the human pelvis." FAA-AM-82-9, Technical Report, U.S.Dept of Transportation, FAA, Office of Aviation Medicine, Washington, D. C., 20591, 1982.
[43] Brodeur RR, Reynolds HM. "Initial position and postural attitudes of driver occupants: Modeling spinal curvature." ERL-TR-95-007, Technical Report, Ergonomics Research Laboratory, Michigan State University, East Lansing, 1996.
[44] Garcia M, 1994. Reconstruction of visual surfaces from sparse data using parametric triangular approximants, *IEEE ICIP*, pp. 750-754.
[45] Akima H, 1978. A method of bivariate interpolation and smooth surface fitting for irregularly distributed data points, *ACM Trans. on Mathematical Software*, vol. 4, pp. 148-159.
[46] Cui Y and Weng J, 1995. Reconstructing and visualizing dense global visual maps for extended passive navigation, *Proceedings of SPIE Conference on Visual Data Exploration and Analysis II*.
[47] Beckman P, 1973. *Orthogonal Polynomials for Engineers and Physicists*, Golem, Boulder, CO.
[48] Haralick R, Shapiro L, 1992. Computer and robot vision, Addison, Wesley, pp 394-396.
[49] Chow W and Odell E, 1978. Deformations and stresses in soft body tissues of a sitting person. J Biomech Eng, 100:79-87.
[50] Michlin S and Smolickii H, 1967. *Approximate Methods for Solution of Differential and Integral Equations*, New York: Elsevier.

[51] Zenisek A, 1970. Interpolation polynomial on the triangle, *Numer. Math.*, vol. 15, pp. 283-296.

Appendix A

Kernels for estimating the coefficients k_1, k_2,...,k_{10}.

1	1	1	1	1
1	1	1	1	1
1	1	1	1	1
1	1	1	1	1
1	1	1	1	1

k_1

2	-1	-2	-1	2
2	-1	-2	-1	2
2	-1	-2	-1	2
2	-1	-2	-1	2
2	-1	-2	-1	2

k_6

-2	-2	-2	-2	-2
-1	-1	-1	-1	-1
0	0	0	0	0
1	1	1	1	1
2	2	2	2	2

k_2

-1	-1	-1	-1	-1
2	2	2	2	2
0	0	0	0	0
-2	-2	-2	-2	-2
1	1	1	1	1

k_7

-2	-1	0	1	2
-2	-1	0	1	2
-2	-1	0	1	2
-2	-1	0	1	2
-2	-1	0	1	2

k_3

-4	-2	0	2	4
2	1	0	-1	-2
4	2	0	-2	-4
2	1	0	-1	-2
-4	-2	0	2	4

k_8

2	2	2	2	2
-1	-1	-1	-1	-1
-2	-2	-2	-2	-2
-1	-1	-1	-1	-1
2	2	2	2	2

k_4

-4	2	4	2	-4
-2	1	2	1	-2
0	0	0	0	0
2	-1	-2	-1	2
4	-2	-4	-2	4

k_9

4	2	0	-2	-4
2	1	0	-1	-2
0	0	0	0	0
-2	-	0	1	2
-4	-2	0	2	4

k_5

-1	2	0	-2	1
-1	2	0	-2	1
-1	2	0	-2	1
-1	2	0	-2	1
-1	2	0	-2	1

k_{10}

Appendix B

Discretization Error

In this section, we estimate the discretization error to show the convergence of the method for smoothing the pressure mapping of the coarse-grid large Tekscan mat. For the sake of brevity we restrict ourselves to the Dirichlet problem for the biharmonic equations:

$$\Delta^2 u = f(x_1, x_2), (x_1, x_2) \in \Omega \tag{B.1}$$

$$u|_\Gamma = \left.\frac{\partial u}{\partial v}\right|_\Gamma = 0 \tag{B.2}$$

However, the results still hold for other boundary conditions. The solution $u(x_1, x_2)$ of the Dirichlet problem minimizes the functions

$$F(v) = \int_\Omega [A - 2 f(x_1, x_2) v] dx \tag{B.3}$$

in the class $W_2^{(2)}(\Omega)$, where

$$A = \left(\frac{\partial^2 v}{\partial x_1^2}\right)^2 + 2\left(\frac{\partial^2 v}{\partial x_1 \partial x_2}\right)^2 + \left(\frac{\partial^2 v}{\partial x_2^2}\right)^2$$

and $W_2^{(k)}(\Omega)$ means the Sobolev space of functions having generalized derivatives up to order k [50].

Let $H_5(\Omega)$ be the class of functions defined on $\overline{\Omega}$ which on the particular triangles of the given triangulation are equal to the polynomials [45]. The approximate solution $U(x_1, x_2)$ is defined as that function from H_5 which minimizes the functions [49] in the class H_5. To find an estimate for the discretization error, we introduce the notation

$$J_0(z) = \int_\Omega \left[\left(\frac{\partial^2 z}{\partial x_1^2}\right)^2 + 2\left(\frac{\partial^2 z}{\partial x_1 \partial x_2}\right)^2 + \left(\frac{\partial^2 z}{\partial x_2^2}\right)^2\right] dx \tag{B.4}$$

Then it holds (see Michlin and Smolickii [50])

$$\begin{aligned} J_0(U - v) &= F(U) - F(v) \\ &= \min_{v \in H_5} J_0(v - u) \\ &\le J_0(u - \tilde{u}) \end{aligned} \tag{B.5}$$

where $\tilde{u}$ is the function from H_5 such that the values of $\left|D^i\tilde{u}\right|$ for $|i| \le 2$ at the vertices of the triangles and the same as those of the solution $u(x_1, x_2)$. Here $\left|D^i u\right| = \frac{\partial^{|i|}|_u}{\partial x_1^{i_1} \partial x_2^{i_2}}$ and $|i|=i_1+ i_2$. Assume u has bounded derivatives of the sixth order in the interior of T,

$$|D^i u| \le C, \quad |i| = 6 \tag{B.6}$$

We have an estimate (see Zenisek [51])

$$\left[J_0(u - \tilde{u})\right]^{1/2} = O\left(\frac{Ch^4}{\sin^2 \alpha}\right) \tag{B.7}$$

where h is the largest side and α is the smallest angle of all triangles of the given triangulation. Equation (B.7) means that if we refine the triangulation in such a way that $\alpha \ge \alpha_0 > 0$ the approximate solution converges to the exact solution.